

SACLANTCEN MEMORANDUM
serial no.: SM-234

*SACLANT UNDERSEA
RESEARCH CENTRE*

MEMORANDUM



**Oceanographic analysis
of NAPOLI '85,
an experiment in the Tyrrhenian Sea**

J.R. Potter

March 1990

The SACLANT Undersea Research Centre provides the Supreme Allied Commander Atlantic (SACLANT) with scientific and technical assistance under the terms of its NATO charter, which entered into force on 1 February 1963. Without prejudice to this main task – and under the policy direction of SACLANT – the Centre also renders scientific and technical assistance to the individual NATO nations.

This document is released to a NATO Government at the direction of SACLANT Undersea Research Centre subject to the following conditions:

- The recipient NATO Government agrees to use its best endeavours to ensure that the information herein disclosed, whether or not it bears a security classification, is not dealt with in any manner (a) contrary to the intent of the provisions of the Charter of the Centre, or (b) prejudicial to the rights of the owner thereof to obtain patent, copyright, or other like statutory protection therefor.
- If the technical information was originally released to the Centre by a NATO Government subject to restrictions clearly marked on this document the recipient NATO Government agrees to use its best endeavours to abide by the terms of the restrictions so imposed by the releasing Government.

Page count for SM-234
(excluding covers)

Pages	Total
i-vi	6
1-38	38
	<hr/> 44

SACLANT Undersea Research Centre
Viale San Bartolomeo 400
19026 San Bartolomeo (SP), Italy

tel: 0187 540 111
fax: 0187 560 770
telex: 271148 SACENT I

NORTH ATLANTIC TREATY ORGANIZATION

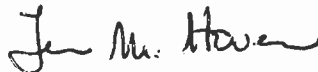
SACLANTCEN SM-234

Oceanographic analysis
of NAPOLI '85,
an experiment in
the Tyrrhenian Sea

J.R. Potter

The content of this document pertains
to work performed under Project 05 of
the SACLANTCEN Programme of Work.
The document has been approved for
release by The Director, SACLANTCEN.

Issued by:
Underwater Research Division



J.M. Hovem
Division Chief

SACLANTCEN SM-234

**Oceanographic analysis of NAPOLI '85,
an experiment in the Tyrrhenian Sea**

J.R. Potter

Executive Summary: The performance of all sonar systems is affected by variability in the sound speed of the ocean medium along the acoustic transmission path. This variability may increase or decrease the received signal strength by some ± 10 dB, resulting in anomalously high or low detection ranges. In order to explore the possible gains that such variability may offer, and the limits imposed on sonar equipment, the variability in the medium must be first understood. Only with environmental input can the advanced relevant acoustic propagation models and propagation theory be used to realistically predict sonar performance.

NAPOLI '85 was an acoustic-oceanographic experiment conducted in the Tyrrhenian Sea with the objective of simultaneously measuring acoustic propagation and the intervening transmission medium between source and receiver. Some acoustic results were presented in SACLANTCEN Memorandum SM-223. This memorandum presents the physical oceanographic analysis, which provides the relevant input parameters for acoustic theory. It has been found that the sound-speed inhomogeneities were predominantly caused by isolated regions, or 'glob's' of cooler, less saline water embedded in a warm, salty background water mass caused by imperfect mixing of Atlantic inflow waters with older saltier Mediterranean waters. The size of these 'glob's' was typically some 4 km long \times 40 m thick. Internal waves in the ocean, very often assumed to be the primary source of variability, were of insignificant strength. Oceanographic data analysis techniques and a simple model have been developed to describe the ocean variability and reduce the environmental data to useful parameter values for input to theory.

Further development of the 'glob' model is underway, describing the spatial properties more accurately. It may be possible to develop a simple, empirical environmental model which can represent the observed ocean structure and which provides a simple interpretation of relevant vertical and horizontal scale sizes. This would provide values directly suitable for input to range-dependent acoustic models.

**Oceanographic analysis of NAPOLI '85,
an experiment in the Tyrrhenian Sea**

J.R. Potter

Abstract: In 1985, an acoustic/oceanographic experiment (NAPOLI '85) was carried out in the Tyrrhenian Sea to investigate acoustic propagation variability due to inhomogeneities in the ocean medium. In order to provide input parameters for the acoustic theory, the oceanographic medium must be characterised and it is this work which is presented. Data are analysed from thermistor chains, XBT's, CTD's and (most importantly) a towed oscillating body (TOB) with CTD sensors. The TOB allows ocean properties to be mapped in the vertical-horizontal plane. These maps show significant oceanic sub-meso scale features (typically 4 km long \times 40 m deep) which are tracked through 10 TOB casts over a three-day period.

A procedure for separating internal-wave activity from finestructure is developed and applied. This procedure provides a means to classify the source mechanism for the variability, and hence determine the appropriate treatment. The ocean variability is found to have been almost entirely caused by advective intrusions, with very little internal-wave activity. An internal-wave model is applied to the separated wave field and is shown to agree moderately well. The model cannot be made to match the finestructure field, which has a $\beta^{-5/2}$ horizontal wavenumber spectrum. Characteristic length-scale definitions are developed and evaluated for the horizontal and vertical directions. The horizontal length scale is ~ 2 km and is depth-invariant. Vertical scales vary from 7 to 50 m over the depth range 50–400 m, respectively. The sound-speed variance has a complicated depth-dependence which can be related to the observed oceanographic intrusions.

Keywords: acoustic variability \circ globs \circ internal waves \circ models \circ Napoli \circ ocean variability \circ propagation \circ sonar performance \circ sound speed \circ Tyrrhenian Sea \circ wave spectra

Contents

1. Introduction	1
2. Physical oceanographic data analysis	4
2.1. <i>Thermistor chain data</i>	5
2.2. <i>CTD data</i>	5
2.3. <i>XBT data</i>	9
2.4. <i>TOB data</i>	11
3. Dynamical oceanographic data analysis	18
3.1. <i>Principle of separation of internal-wave effects</i>	18
3.2. <i>Application of an internal-wave model</i>	20
3.3. <i>Experimental results of separation</i>	21
3.4. <i>Examination of horizontal wavenumber spectra</i>	22
4. Environmental characterisation	25
4.1. <i>Length scales, autocorrelation and structure functions</i>	26
4.2. <i>Measurements of $\langle \mu^2 \rangle$, the averaged sound-speed variance</i>	32
5. Conclusions	36
References	37

Acknowledgement: This work was made possible by the energies of T. Akal and B. Uscinski, who designed the NAPOLI '85 experiment and, together with the staff of SACLANTCEN and the author, carried it out. Special thanks to Enzo Michelozzi, who always manages to make something work, and Tom Hopkins, who contributed ideas and helped iron out some of the bumps in my physical oceanography.

1

Introduction

Since 1985, the acoustic propagation research performed under project 05 has been performed in collaboration with the Department of Applied Mathematics and Theoretical Physics (DAMTP) at Cambridge, UK, to investigate fluctuations in acoustic propagation due to random inhomogeneities in the ocean medium. This work applies modern multiple scattering theory [1] to the ocean medium in order to characterise the resulting stochastic properties of fluctuations in sound propagation. In October 1985 an experiment, known as NAPOLI '85, was carried out in the central Tyrrhenian Sea (Fig. 1), which simultaneously measured the acoustic propagation of a broadband source over a fixed geometry and properties of the ocean volume environment. An analysis of the acoustic results showed that the relative arrival time measured in the vertical exhibited fluctuations both in space and time, caused by sound-speed variations in the ocean [2]. A statistical description of the ocean medium is required as input to the scattering theory in order to obtain quantitative theoretical results for comparison with the acoustic observations. It is this description which forms the basis of this memorandum.

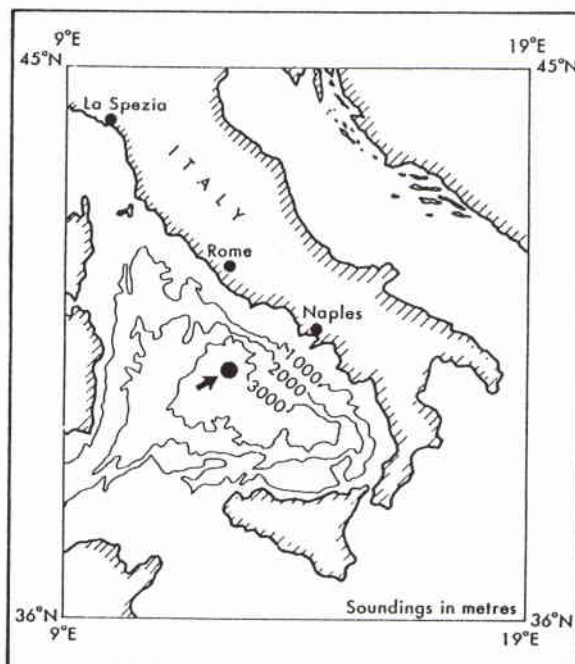


Figure 1 Location of the experiment in the Tyrrhenian Sea, indicated by an arrow. The local bathymetry is shown with 1000 m contour intervals.

The major part of the oceanographic data consists of temperature, conductivity and pressure measurements made by a towed oscillating body (TOB). The TOB is a device that carries standard CTD sensors but which is towed behind a ship [3]. The TOB is made to oscillate in depth between two pre-set limits while the towing ship moves forward, thus the sensors describe a 'zig-zag' path in the vertical. The TOB was towed by the Italian research vessel *Magnaghi* in a cruciform pattern, along the acoustic transmission track and then perpendicular to it. The data can be used to construct two-dimensional sections of the ocean medium, some 270 m deep and several kilometres long. There are 14 of these TOB casts, of which 10 have a length over ~ 10 km. Preliminary analysis of these data showed some interesting small-scale oceanographic features [4].

There are 7 CTD casts, made periodically from the *Maria Paolina G.* (MPG) as opportunity allowed, which provide accurate data over a greater depth range. Supporting XBT casts were also made from the MPG, of which there are ~ 70 . Finally, two thermistor chains were moored at either end of the acoustic transmission path.

In order to quantitatively evaluate the acoustic multiple scattering theory, we require the autocorrelation function (a.c.f.) in space and time of the stochastic sound-speed inhomogeneities. For this purpose, it is easiest to assume that internal waves are the major contributor to inhomogeneities in the sound speed of the medium. Many acoustic fluctuation studies, such as Williams [5], have been analysed extensively in terms of internal wave theory, usually invoking the very successful formulation of Garrett and Munk [6]. Williams [5] had sufficient environmental data to demonstrate that non-internal-wave effects were indeed insignificant for his data.

Internal waves are governed by well-defined spatial and temporal relationships. Internal wave theory is well developed and provides fairly reliable predictions from rather limited data. The functional forms of the wavenumber spectra and other expressions required as input to the scattering theory have already been developed for internal waves and may easily be applied [7]. For some experiments, internal waves are indeed the major contributor to the sound-speed variability (such as for the Cobb data presented in [8] and data from the Gulf of Cadiz discussed in [9]. In a few other experiments, internal waves contribute perhaps only half of the variability (for example, the low vertical wavenumber data from MATE [10]). In the NAPOLI '85 experiment, we shall show that internal waves provide a negligible contribution. In such a situation, the variability is provided by advection, up- and down-welling and the generation of regions of water each having different sound speeds, which are then modified by turbulence, diffusion etc. We shall concern ourselves here only with small-scale features (< 10 km). The whole set of these features and processes is often described by the umbrella term 'finestructure'. This definition is based on scale, not the originating physical process.

Finestructure causes sub-meso (typically 1–50 m deep \times 0.1–5 km long) scale regions in the body of the ocean with anomalous sound speeds which scatter the sound. Of

SACLANTCEN SM-234

course, disturbances occur over much larger and smaller scales, but it is the sub-meso scale which is relevant to acoustic frequencies above 30 Hz (lower frequencies do not 'see' variability of 50 m or less, due to diffraction effects) over propagation ranges of ~ 10 km. Inhomogeneity scales larger than 5 km in the horizontal will be largely accounted for by the mean, deterministic profile. These 'globs', as we shall call them, need not obey any convenient rules about motion, size or shape since they may have the same density as the surrounding water. Indeed, this is the most stable (and therefore likely) situation, since globs which are not density-compensated will tend to rise or sink to their in-situ density level and become density-compensated, or decay rapidly in time by mixing, driven by the unstable potential energy. Density-compensated globs decay only through relatively slow processes, such as diffusion. The behaviour of a density-compensated glob is governed by external forces, such as the background motion, shear distortion etc. and the glob may take any number of shapes and forms. In cases where internal waves are not the primary contributor to sound-speed inhomogeneities, many more environmental data must therefore be collected in order to characterise the medium. A considerable portion of the following analysis will deal with a procedure to identify the extent of non-internal-wave contributions to sound-speed inhomogeneities and the development of procedures to characterise the medium which are valid irrespective of the type.

The reader is reminded that these environmental data were collected in support of an acoustic transmission experiment. For this reason, both the data collection and their analysis are in terms of the parameters of direct acoustic importance. The traditional physical and dynamic oceanographic analyses are used only when the results are directly relevant as input to the acoustic scattering theory. The scale sizes of the data are much smaller than for traditional oceanographic surveys. In the absence of internal-wave-dominated inhomogeneities, the TOB data are then the only data type which allows the calculation of the statistics relevant to the acoustic theory, since data are required with a resolution in both the horizontal and vertical sufficient to resolve sub-meso scale features. Prominence is therefore given to the TOB data, with a correspondingly sparse treatment of CTD, XBT and thermistor chain data.

2

Physical oceanographic data analysis

This section will present the basic data collected from thermistor chain, CTD, XBT and TOB systems and discuss the results achieved from a preliminary physical oceanographic analysis. The most complete understanding of the ocean medium during the experiment is obtained in a later section by integrating all the information, playing off the various advantages and limitations of each type of data taken in isolation.

The disposition of the various sensors is shown schematically in Fig. 2.

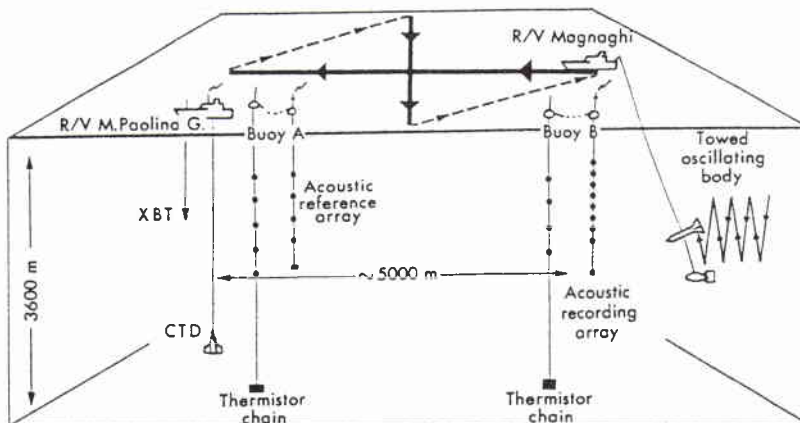


Figure 2 Schematic representation of the environmental sensor distribution. The TOB was towed in a cruciform pattern parallel, and then perpendicular to the acoustic propagation track.

SACLANTCEN SM-234**2.1. THERMISTOR CHAIN DATA**

Figure 2 shows the positions of the two thermistor chains, each with 10 thermistors. The thermistors were sampled at 5 min intervals for the period 273–282 (Julian day), starting before the main experiment and continuing until afterwards. The thermistor chain records are the longest (in time) of all the environmental records. The chains covered the depth range 216–306 m, with the thermistors placed at regular 10 m intervals. The digital resolution of the recorded temperatures is 0.025°C. Unfortunately, the thermal variability in the 200–300 m range was only of the order of 0.04°C. This meant that the fluctuations were barely resolved by the thermistor recordings. Many thermistors experienced a total range of temperatures over the 9 days spanning only 4 digitisation intervals. The thermistor data are thus not very useful for anything but the most crude analysis. All the data (after cutting data errors) for one of the two chains are displayed in Fig. 3. Perhaps the strongest conclusion that can be drawn from these data is that the general level of temperature fluctuations is of the order of 0.05°C and that there is no strong depth dependence.

2.2. CTD DATA

A total of 7 CTD casts were made during the experiment. The Julian dates of the casts are given in Table 1.

Table 1 *CTD casts*

Cast no.	Julian date
1	267
2	269
3	269
4	273
5	279
6	280
7	281

Casts 1–3 were taken before the main body of the acoustic experiment and therefore before the other environmental data were collected. Casts 4–7 were taken during the main environmental and acoustic acquisition period and are therefore more useful for comparison with other data.

The CTD casts provide the most accurate data and cover the entire depth range of interest (0–400 m) and beyond. The primary use of these data is in characterising the mean background water types and structure of the water column. Their limitation is that there are too few of them to perform useful statistics for characterising the

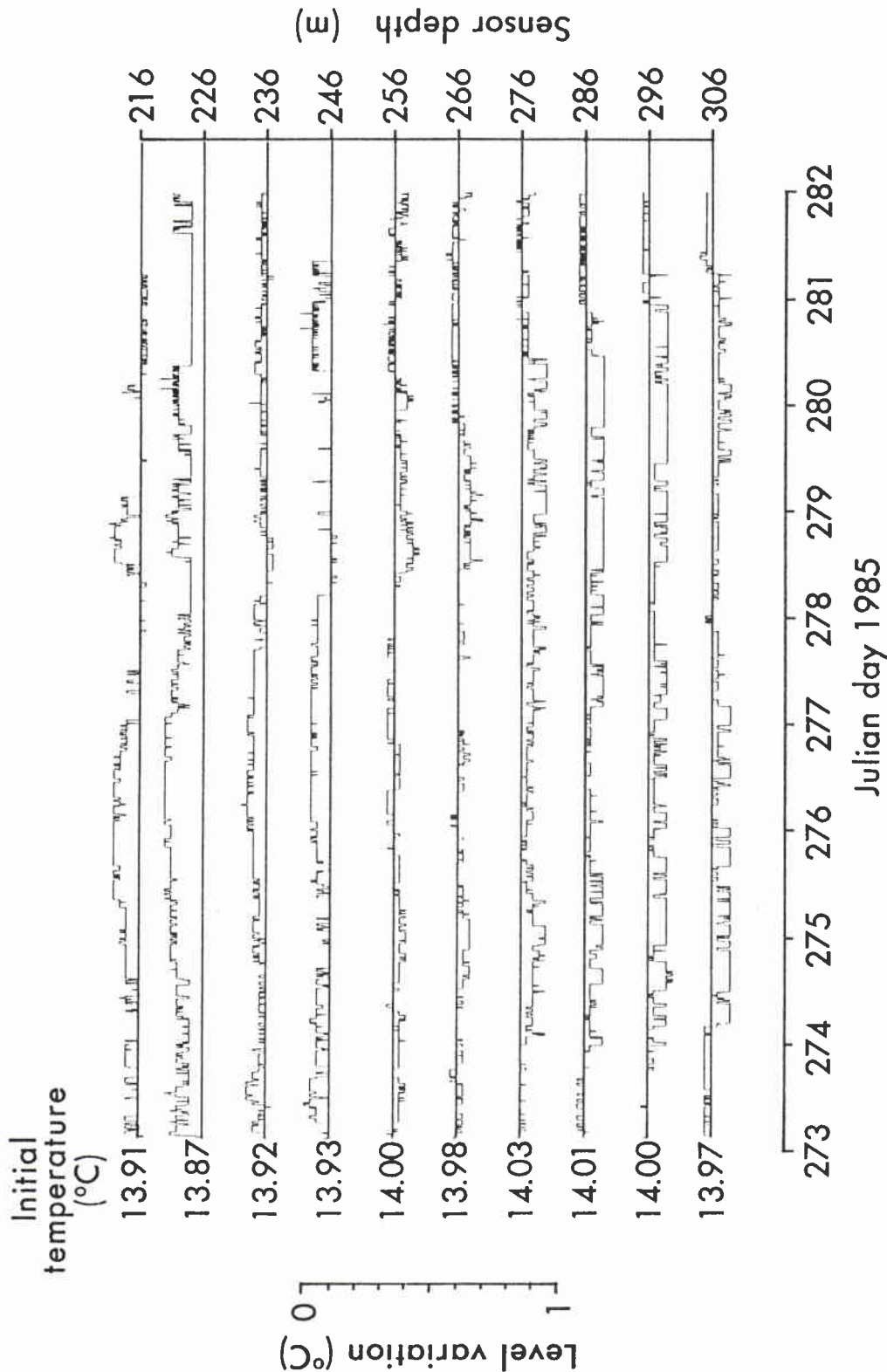


Figure 3 One of the two thermistor chain records for the entire 9 days, along the x-axis, for all 10 thermistors, shown separated along the y-axis. The temperature scale and starting temperatures for the thermistors are shown on the left-hand scales. The thermistor depths are shown on the right-hand scale.

SACLANTCEN SM-234

stochastic properties of the ocean medium. The sound-speed profiles for casts 1–3 are shown in Fig. 4a and those for casts 4–7 in Fig. 4b.

Both Figs. 4a and b show the distinct double-diffusive interfaces below 600 m depth characteristic of this region [11], although only 6 such layers are observed as opposed to the 10 monitored by Molcard and Tait over a 2.5-year period [12]. Examination of the potential density profile confirms that the water column is almost neutrally stable below 600 m, with an extremely small mean vertical potential density gradient of $3 \times 10^{-5} \text{ kg m}^{-4}$ over the range 500–1800 m. The potential density is strictly monotonic increasing with depth, with no significant steps or fluctuations. The potential density variance below 250 m is always less than $5 \times 10^{-6} \text{ kg}^2 \text{ m}^{-6}$, which is so low that it may be limited by the noise of the CTD measuring system. The observed depth of the double-diffusive interfaces varied from one profile to another by as much as 50 m, perhaps in response to motion induced by internal waves at these depths. Each interface can be tracked from one CTD cast to the next. There is no evidence of a progressive change in the depths of the interfaces with time.

The interfaces generally have a single step in salinity and temperature occurring over a depth of 2.5 m or less. Some interfaces consist of two steps, closely spaced, which sometimes unite into only one step, or vice versa. It seems that it is possible for a salinity/temperature step to split into two steps, separated by an intermediate layer 10 m or more deep, which then reverts back to a single step once again some time later. This may be an example of salt-finger interface instability which numerical experiments have shown can give rise to large oscillations of the interface (N. Brummel, personal communication). The steps in salinity and temperature are of the order of 0.035 p.p.t. and 0.15°C , respectively, tending to become less with increasing depth. These step values are some 50% larger than those found by Molcard and Tait, as one would expect since there are fewer layers. The total change in salinity and potential temperature from 600 to 1900 m is thus very similar. The long term evolution of the layers studied by Molcard and Tait during 1972–1974 has thus been a coalition of some layers to form fewer, but more marked, steps over the last 10 years.

In order to characterise the water types and set the environment in context of the larger-scale circulation of the Tyrrhenian basin, it is useful to examine the T – S curves, the plot of temperature against salinity with depth. Each water type has a characteristic temperature and salinity, and is therefore identified by a unique point in the T – S diagram. The T – S curves for CTD casts 1–3 and 4–7 are shown in Figs. 5a and b. Both figures are annotated with local minimum and maximum values of temperature and salinity, since all other water masses can be generated by mixtures of water with local extreme values of T and S . The extrema therefore identify the source water types. The following identification of the source waters comes from an analysis of the larger-scale physical oceanography by Hopkins and Zanasca [13]. The local salinity minimum S_{\min} is due to incoming Atlantic surface water (ASW). The warmer, more saline water above 30 m depth is produced by

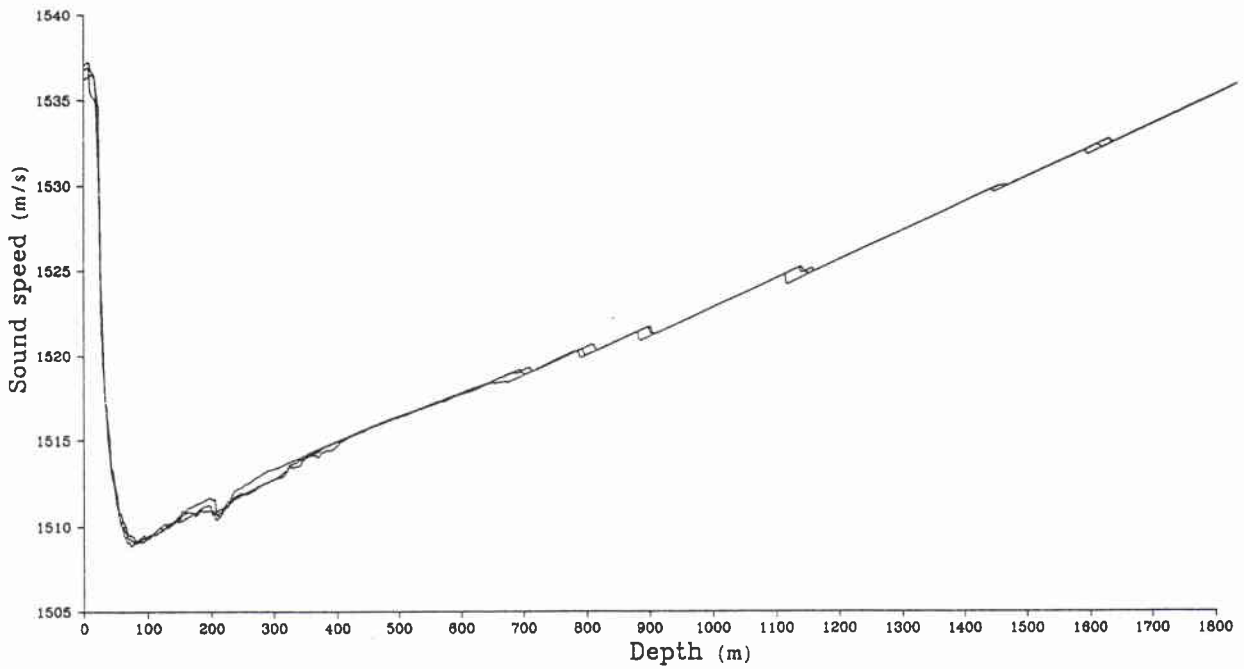


Figure 4a Sound-speed profiles for CTD casts 1-3, taken before the acoustic experiment and TOB data collection.

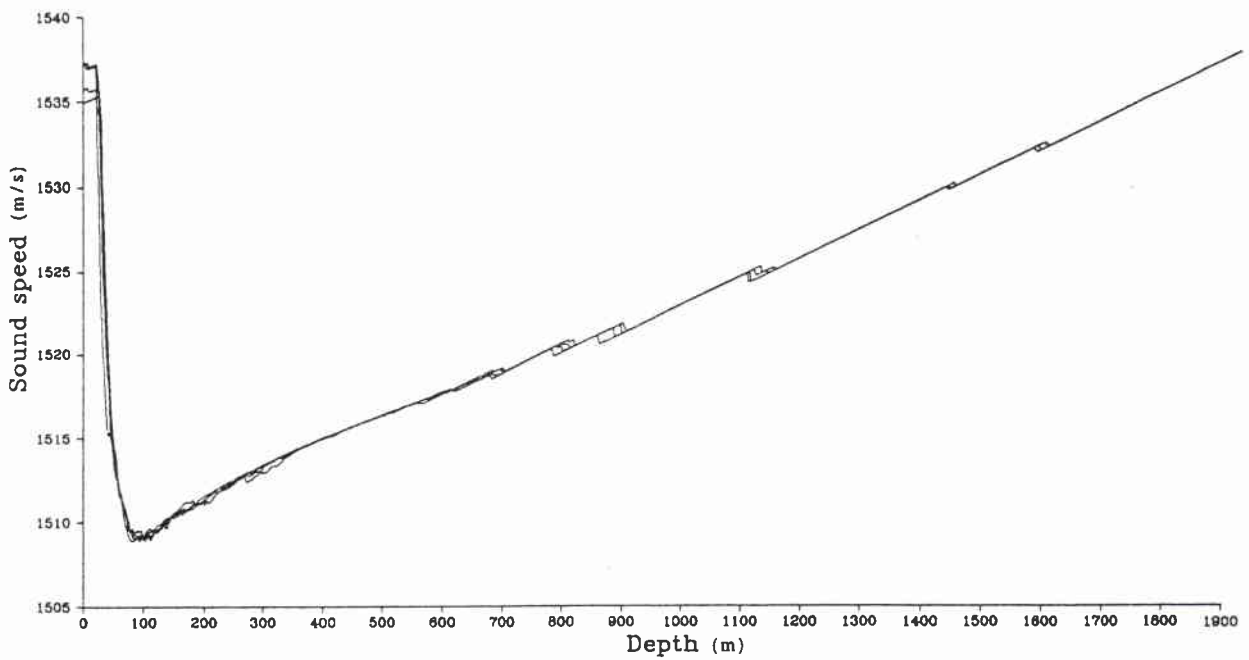


Figure 4b Sound-speed profiles for CTD casts 4-7, taken during the acoustic experiment and TOB data collection.

SACLANTCEN SM-234

solar heating and evaporation of the surface Atlantic inflow. T_{\min} is a remnant of winter water, cooled by lower winter air temperatures and mixed downward by winter storms. By October, this minimum is almost completely overrun by the warmer waters above and below. T_{\max} and S_{\max} are associated with Levantine intermediate water (LIW) from the eastern Mediterranean. All the observed values are in agreement with the more broadly applicable findings of Hopkins and Zanasca [13] from their survey.

Comparison of Figs. 5a and b shows that sometime between CTD casts 1–3 and 4–7, a significant input of ASW occurred, lowering the salinities at 30 m depth by as much as 0.15 p.p.t. Figure 5b shows a corresponding increase in inter-cast variability at this depth. At ~ 220 m depth, Fig. 5a shows a strong intrusion of cooler, less saline water, whose origin is not known. No neighbouring water mass in the column has the observed T – S values and so it appears most likely that this intrusion is a detached remnant of some Atlantic inflow that has been greatly modified and has had time to sink or rise to its equilibrium depth. CTD casts 4–7 also show some cool, low salinity intrusions between 200 and 400 m depth, but they are much less pronounced and are thicker in the vertical.

2.3. XBT DATA

A total of 72 XBT's were taken during the period 277–279 (Julian day) at varying intervals between 15 min and 1 h. As is typical of these devices, a rather high number of them were faulty in one way or another. After cutting faulty data, 59 XBT casts remained. The digital recording interval and basic resolution of the XBT's are in the region of 0.02°C , only slightly better than for the thermistor chains. The data are much more useful, however, because they were collected over the whole depth range of interest, 0–400 m. A plot of all the XBT data, after cutting, is shown in Fig. 6.

The XBT device tends to have a rather poor absolute accuracy, but rather better resolution. There are a number of ways in which the quality of information provided by the casts can be improved. The most effective in this case turned out to be a 'calibration' using the CTD data which have a good resolution and absolute accuracy. The CTD casts all showed a very stable value for temperature at a depth of 450 m, with a potential temperature variance (for the 4 casts taken around the period of the XBT casts) of only $2 \times 10^{-5}^{\circ}\text{C}^2$. This is equivalent to an rms variability in the potential temperature at 450 m of less than 0.005°C , which may have been the lower limit of the CTD instrument noise. A bias was applied to each XBT cast to set the XBT potential temperature value at 450 m equal to the mean value from the CTD casts. The absolute calibration of the XBT casts was thus improved to 0.005°C , the measured rms temperature variability at 450 m.

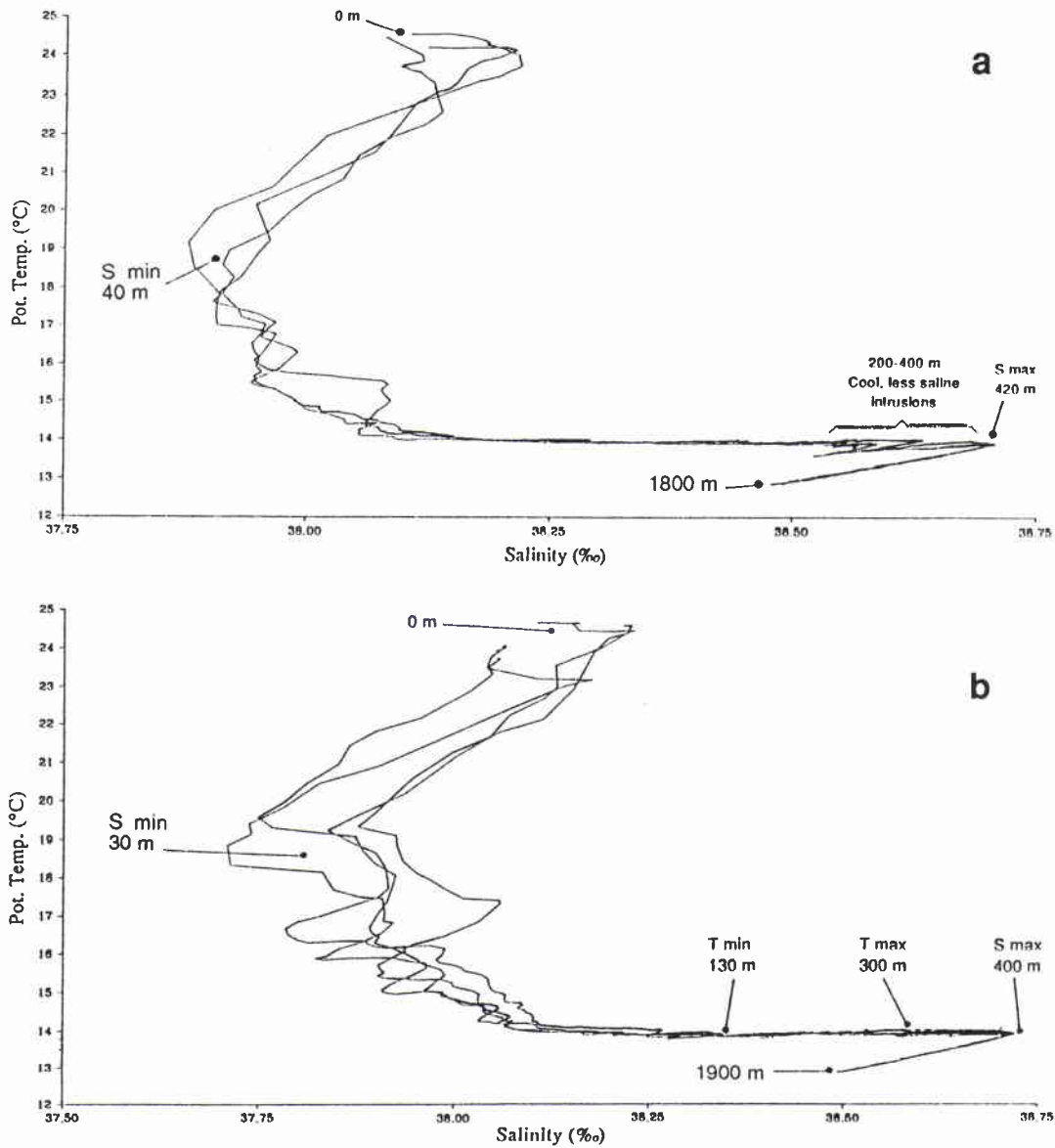


Figure 5 *T-S* curves for (a) CTD casts 1-3, and (b) CTD casts 4-7. The depths and positions of minimum and maximum temperature and salinity are shown beside the curves.

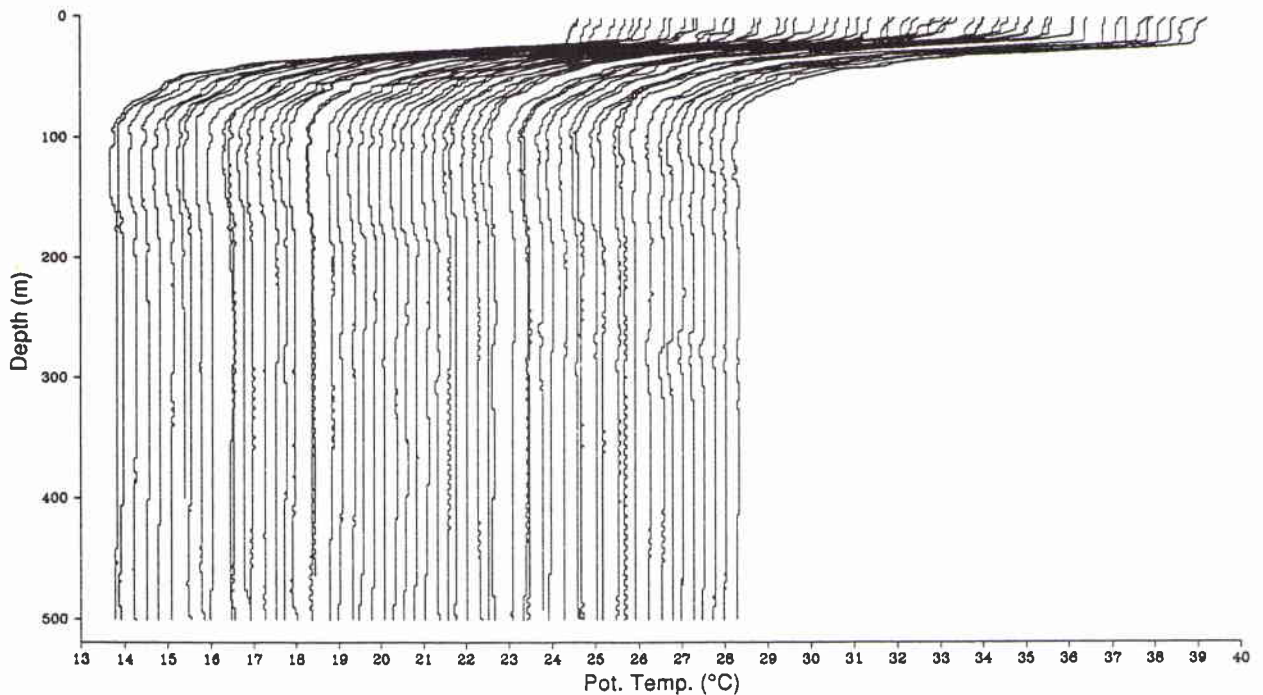
SACLANTCEN SM-234

Figure 6 XBT data (after cleaning) shown as a series of vertical potential temperature profiles, each offset from the last by a horizontal displacement equal to 0.25°C .

2.4. TOB DATA

The prime advantage of the TOB is its ability to collect data in both the vertical and horizontal, giving a quasi-synoptic 2-D picture of the ocean medium. Such sections allow vertical and horizontal spatial statistics to be evaluated, essential to characterise the ocean medium. The accuracy and resolution of the sensors are the same as for a conventional CTD. The spatial resolution is some 1 m in the vertical and 350 m in the horizontal, on the average. An important output of the TOB data is the production of 'inhomogeneity fields', which are the residual values of a parameter field after the range-averaged mean is subtracted at each depth for a particular cast. Because the other types of environmental data available cannot be used to give 2-D pictures of the transmission medium and hence the statistics required by acoustic multiple scattering theory, only the TOB data will be considered in detail.

In the NAPOLI '85 experiment, 14 TOB casts were made. Of these, 10 casts were of ~ 10 km length or more and were selected for this analysis. The towship and vertical TOB speeds were both ~ 1.5 kn, giving the TOB a 45° track (in the vertical plane) through the water at $\sim 1\text{ m s}^{-1}$. The data were sampled at 12 Hz. The pressure and conductivity data were lagged by 4 samples (equivalent to $\frac{1}{3}$ s) to crudely account for the thermistor time constant. The data were filtered to suppress ship motion and numerical noise, giving output values at 1 m depth interval. No problem was encountered in using both 'up' and 'down' passes of the TOB as with the data from Cadiz [9]. In addition, the filtering scheme used for these data gives a vertical spatial

resolution of 0.5 c.p.m., instead of the 0.07 c.p.m. obtained by Cairns. The sea-state for NAPOLI '85 experiment varied from 0 to 1, much calmer than for most of Cairns' data, which may in part explain the improved data quality.

After data filtering and reduction, the pressure, conductivity and temperature data were converted to give sound speed, salinity, potential temperature and potential density. A further program incorporated the navigational data to give true horizontal distance and interpolated the parameter fields onto a regular grid consisting of cells 75 m long \times 1.5 m deep. The true horizontal resolution of the data varies between $1-2 \times 10^{-3}$ c.p.m., depending on depth, since the 'zig-zag' path gives better resolution at the centre depth of operation than at the extremes. The over-resolution in the horizontal provided by the 75 m interpolation cells was required in order to accurately represent the zig-zag path position and thus correctly place the data at all depths. Those readers interested in more details of the TOB data reduction procedure are referred to the SACLANTCEN Internal Note [4].

The sound-speed data were range-averaged to obtain the mean profile as a function of depth. The residual sound speed was then calculated by subtracting the relevant mean profile value from each datum and interpolating the residuals. The resulting section provides a two-dimensional picture of the sound-speed inhomogeneities which scatter and distort the sound propagation from the mean-field expectation. The residual sound-speed sections for all 10 of the TOB casts selected for analysis are shown in Figs. 7a-j. The cast numbering is chronological. Casts 1, 6, 8, 10 and 12 were taken on overlapping tracks along the transmission path and will be labelled as group 'A' casts. Casts 2, 7, 9, 11 and 13 were taken on overlapping tracks aligned perpendicular to the acoustic transmission path and will be denoted as group 'B' casts. Almost all of the analytic results obtained in the following sections can be qualitatively observed in these sections 'by eye'. High- and low sound-speed inhomogeneities can clearly be seen, with magnitudes exceeding 1 ms^{-1} . Horizontal scales appear to be in the range of 2-4 km. Vertical scales become larger at greater depths, varying from only a few meters to 20 m or so.

Comparing casts within each group shows a high inter-cast correlation. It is possible to identify many features, observed repeatedly in all casts of one or the other group. The lifetime of the observed ocean structure is clearly much longer than the interval between successive casts on the same track. Navigational accuracy and the irregularity of cast intervals makes a detailed analysis unwarranted, but some interesting features can be identified and qualitatively examined. Group A casts show a strong high sound-speed region at 70 m and a weaker, larger mixed feature from 100 to 250 m depth which evolves steadily in time. In addition, there is a thin but persistent high sound-speed feature at 100 m depth, slanted at a true angle of some 0.34° . Strangely, this feature appears to become more clearly defined with time rather than diffusing.

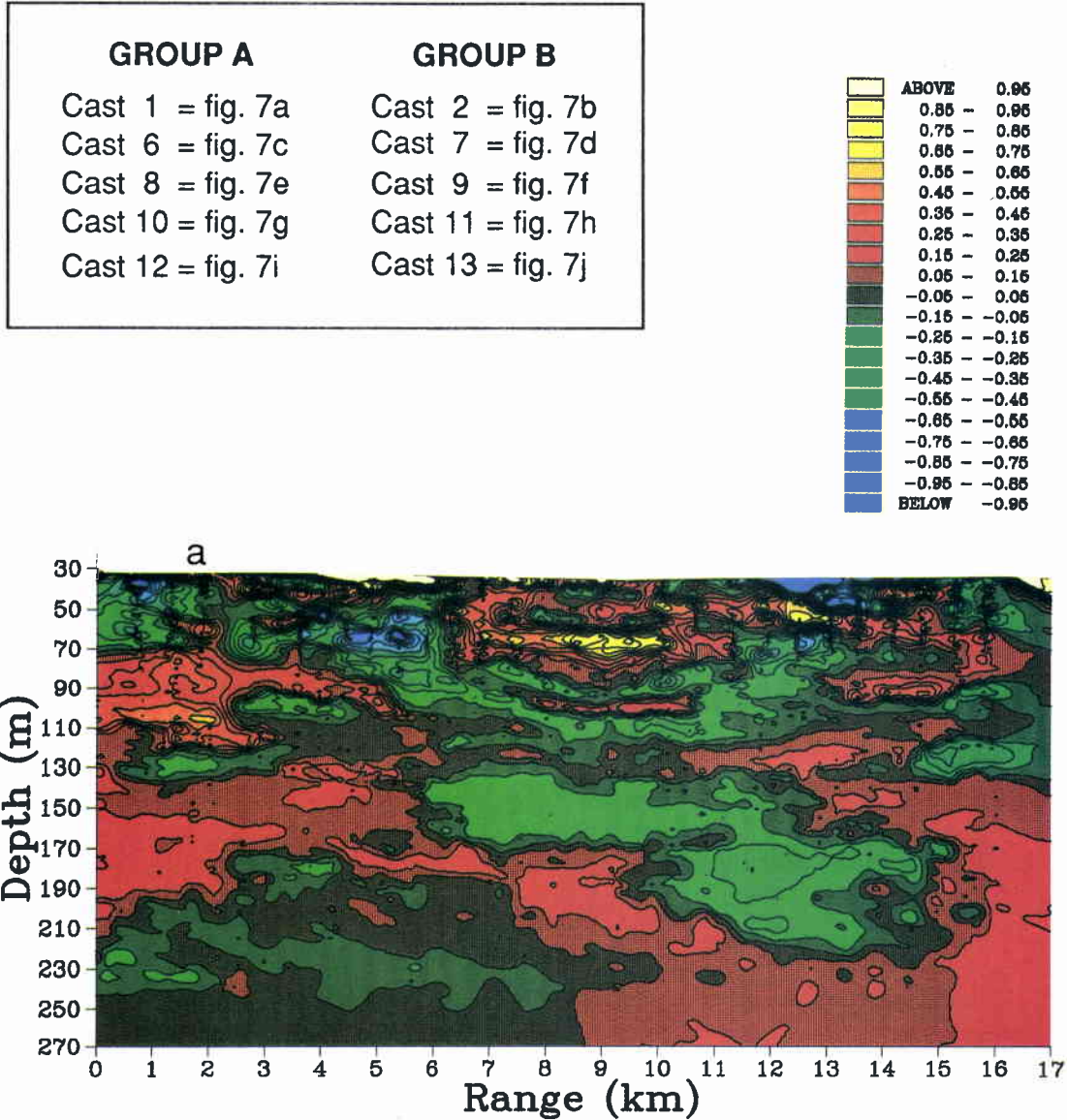
SACLANTCEN SM-234

Group B casts show a different high sound-speed inhomogeneity at 70 m, which almost disappears by cast 13, and a strong, persistent low sound-speed inhomogeneity at ~ 240 m overlain by a weaker, larger higher sound-speed region. The latter feature appears to be some 6 km in length and 30 m thick. Examination of the density fields for these casts shows that these features are density-compensated. Cast 2 shows the deep glob as symmetrical because the towing ship changed course by some 160° at the point marked 9 km on the x -axis, so cutting back through the glob again. Examination of the navigational records reveals that the glob observed in these 5 casts is indeed the same feature, re-sampled on alternate successive TOB casts over a 3-day period. During this period, the glob drifted some 4 km, giving a mean current estimate of 15 mms^{-1} towards 215° T at 240 m depth. The glob can be identified as an example of the low salinity, cool intrusions found in the latter CTD casts, causing a maximum sound-speed anomaly strength of -1 m s^{-1} .

The strength of this glob decays weakly with time, less than halving over the 3-day period. The implied $1/e$ decay time is then in excess of 100 h. Dimensional arguments and the diffusion equation suggest that for a stationary inhomogeneity the $1/e$ decay time should be roughly $l^2/4k$, where l is the minimum length scale and k the diffusivity constant. Johnson and Cox [14] quote a decay time of $l^2/4k\pi^2$ expression based on dimensional argument which has an extra factor of $1/\pi^2$, reducing the above values by a factor of 10. Molecular diffusion is very slow, so that this decay time is either extremely long or the diffusion is turbulent. The turbulent diffusivity is very poorly known, being a function of both the fluid and flow, and estimates for relatively inactive ocean masses vary from $3.7 \times 10^{-5} \text{ m}^2 \text{ s}^{-1}$ [15] to $2 \times 10^{-4} \text{ m}^2 \text{ s}^{-1}$ (Potter, unpublished thesis), implying decay times from 1700 down to 300 h, respectively. In addition to turbulent diffusion, double diffusion may play a role in glob decay. A stability parameter can be evaluated from the Reynolds numbers for heat and salt [16], which indicates that the glob boundaries may develop double diffusive convection. Double diffusion alone could increase the effective diffusion constant to $\sim 10^{-4}$. These estimates are so imprecise that they should be taken only to imply a general consistency with turbulent/double diffusive decay.

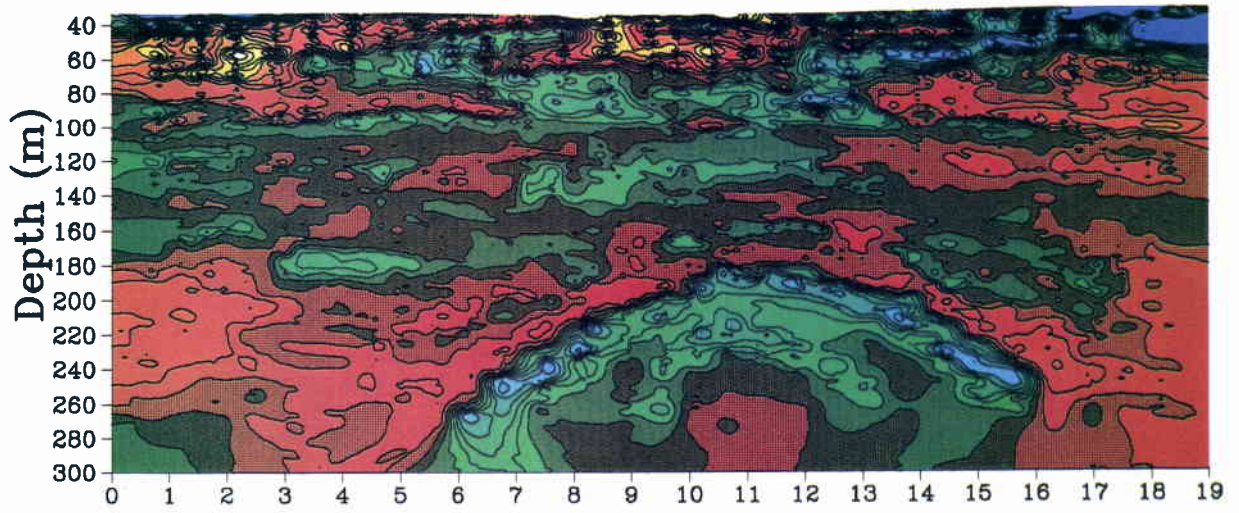
The appearance and (accidental) successful tracking of these globs in a relatively inactive basin spurs interest in further such measurements. Small (10 km or less) inhomogeneities can be found and mapped, providing valuable data not only for interpreting acoustic experimental results but also extending our oceanographic understanding of their spatial and temporal behaviour. Tracking allows the possibility of mean current estimation and investigation of the strength of turbulent diffusion as a function of depth (and hence current strength, column stability etc.). It may be that such inhomogeneities are more profuse than presently assumed, having been swept aside by the successes of internal-wave theory.

Figure 7a-j Residual sound-speed sections for all 10 of the TOB casts used in the analysis. Contour values are given by the accompanying scale in ms^{-1} . Casts 1, 6, 8, 10 and 12 form Group A. Casts 2, 7, 9, 11 and 13 form Group B.

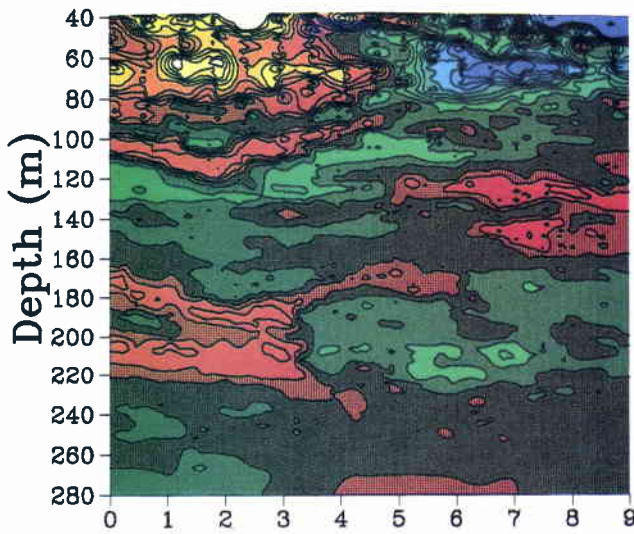


SACLANTCEN SM-234

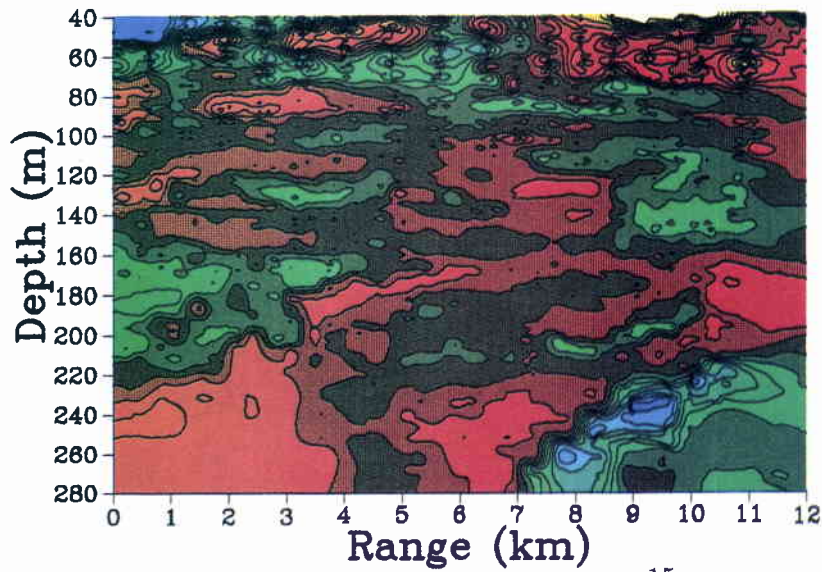
b



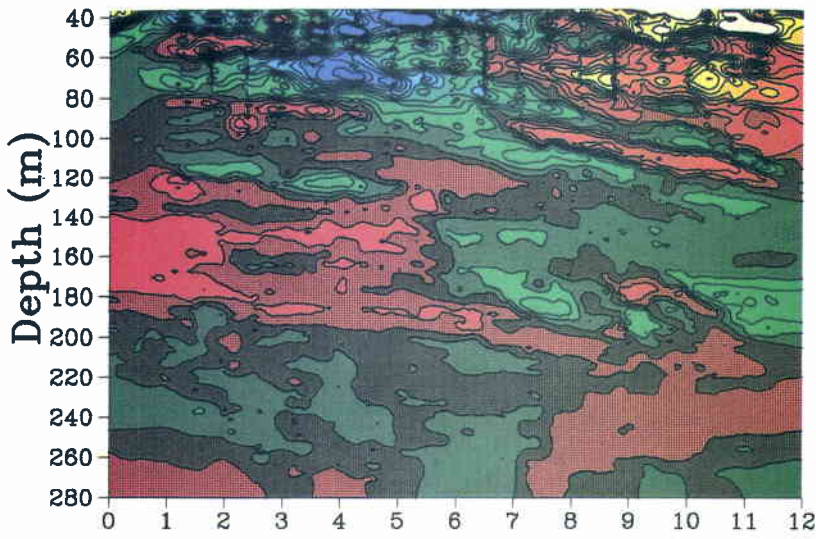
c



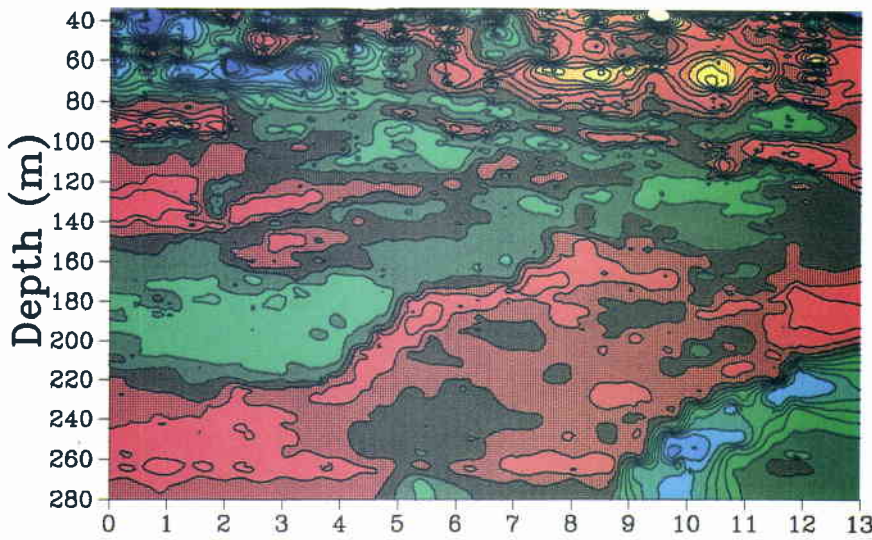
d



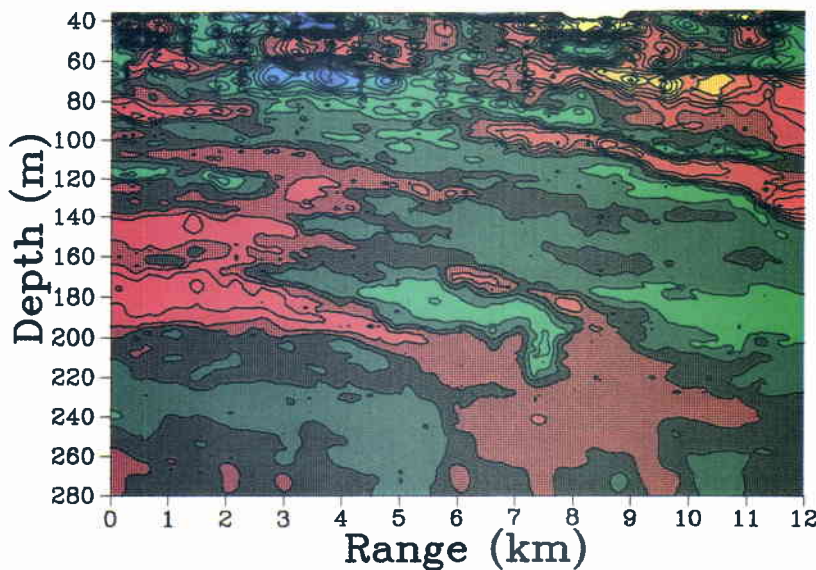
SACLANTCEN SM-234



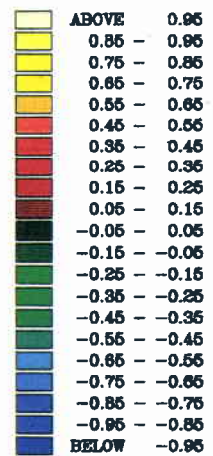
e



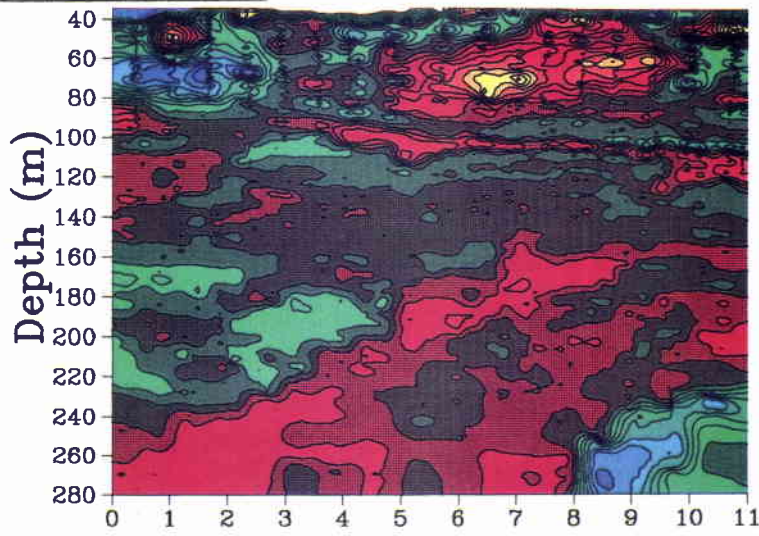
f



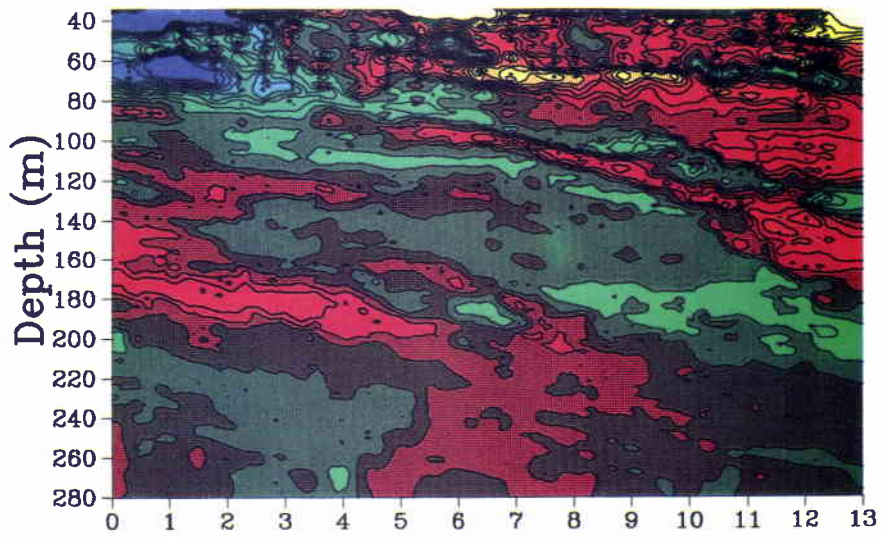
g



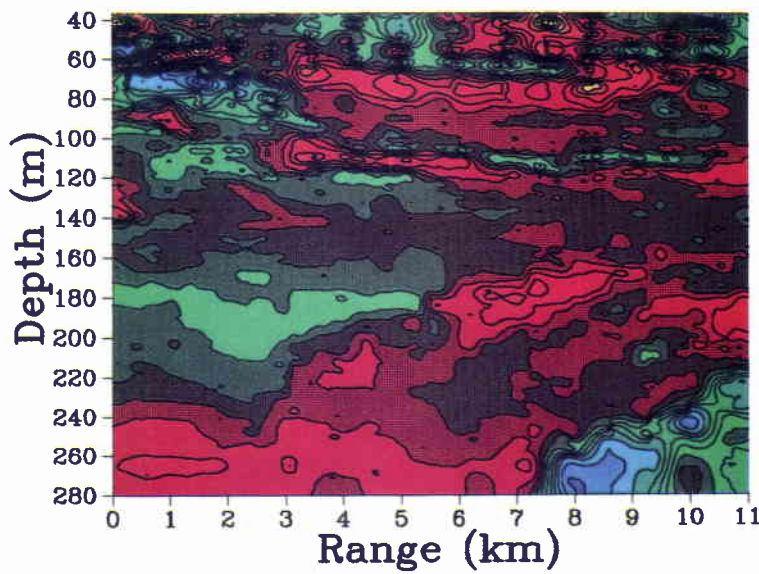
SACLANTCEN SM-234



h



i



j

3

Dynamical oceanographic data analysis

This section discusses the principle and application of a technique to separate internal-wave generated inhomogeneities from finestructure. An internal-wave model is applied for comparison with the separated data. The horizontal wave spectra are examined as a function of depth for both wave- and finestructure-like inhomogeneities.

Our aim is to statistically characterise the inhomogeneities in the sound speed of the medium. This can be done in principle simply by taking exhaustive environmental measurements so that the sound speed is known at all points on the transmission paths at all times during the acoustic experiment, to a resolution sufficient given the wavelength of the acoustic signal. This is clearly prohibitive in practice. An understanding of the dynamics of the ocean can help to augment insufficient environmental data. If the inhomogeneities are of a type controlled by the wave equation together with dispersion relations, such as caused by internal waves, then the information available directly from the data can be extended by use of the appropriate theory. This enables a statistical description of the medium to be built up from very limited data. Before applying internal-wave theory, however, we must be satisfied that internal waves are indeed the governing mechanism. In the absence of extensive environmental data, it may not even be possible to check that internal waves are dominant, and internal-wave theory has to be invoked as an assumption in order to proceed. In the case of the NAPOLI '85 experiment, we have the TOB data, which can be used to evaluate the extent to which internal waves contribute to the inhomogeneities in the medium, at least over the depth range of the TOB data. In order to proceed, we must therefore separate out the internal-wave effects from other contributing mechanisms.

3.1. PRINCIPLE OF SEPARATION OF INTERNAL-WAVE EFFECTS

The residual sound-speed fields displayed in Figs. 7a-j show areas of high and low sound speed which may be due to internal wave displacements, advection, upwelling etc. The sound-speed inhomogeneity field was divided into three classes, following the work of Cairns [9]:

1. Inhomogeneities resulting from the physical distortion of the medium due to internal waves. If there were no inhomogeneities of any sort, then both the density field and the sound-speed field would be range-independent. Internal

waves distort the rest state of the medium, carrying with them the other properties of the medium. The assumption here is that temperature and salinity (and hence sound speed) are 'frozen' tracers in the ocean with respect to internal waves. This is a good approximation given the frequency range of internal waves. Sound-speed inhomogeneities of this type are then directly correlated with inhomogeneities in the potential density field.

2. Inhomogeneities resulting from globs of water with different salinity and potential temperature than the surrounding water which are density compensated. If this were the only type of inhomogeneity, the density field would be horizontally invariant, but the temperature and salinity fields would not be. Inhomogeneities of this type have no correlation with the potential density field. Since this type of inhomogeneity is density compensated, there is not necessarily any significant driving force which forces it to decay. Such a glob may be advected and mixed by the background current field (with its associated turbulent diffusivity), by the development of double diffusive convection (if the heat and salt Reynolds numbers take suitable values) or, in the absence of a more rapid mixing mechanism, the very slow process of molecular diffusion. The lifetime of such a glob varies from a few days to years.
3. Inhomogeneities resulting from globs of water with different salinity and/or potential temperature than the surrounding water which are not density compensated. The evolution of such a glob is driven by its density contrast. If the glob is small, it will move vertically and become a density-compensated glob within the time scale of the buoyancy period (a few hours). If the glob is larger, then it may persist beyond a buoyancy period and in which case will generate some geostrophic current shear due to the induced horizontal pressure gradients. Such a current shear will tend to increase transport across the glob interface by turbulent diffusion and result in a more rapid decay than for a density-compensated glob.

We assume that the third type of inhomogeneity will be rarely observed, because of its short lifetime. Under this assumption, the first two classes can be separated by use of the potential density field. Evaluating the sound-speed field along contours of constant potential density gives the density-compensated glob field. Subtracting this field from the original sound-speed field yields the wave field. Any inhomogeneities of the third type will be lumped together with the wave field. The error in the procedure due to the assumption above thus always leads to an overestimate of the wave field.

3.2. APPLICATION OF AN INTERNAL-WAVE MODEL

Before going on to consider the results of the wave/glob separation, it is convenient to examine the application of internal-wave theory to estimate the horizontal wavenumber spectra of sound-speed inhomogeneities. The basic internal-wave theory used here is the 1975 version of the famous Garrett and Munk model [17]. A convenient formulation of the spectrum is given in [18]; Munk and Zachariasen take linear internal-wave theory and develop an expression for the horizontal wavenumber spectrum assuming a vertically exponential ocean model. The relevant expressions are given in their Eqs. (90) and (93). These expressions evaluate the spectrum for sound-speed inhomogeneities as a function of mode j and horizontal wavenumber β . The equations have been re-arranged to obtain the result in terms of the refractive index variance $\langle \eta^2 \rangle$ so that the expression for the spectrum becomes

$$\frac{4f_I \langle \eta^2 \rangle \beta^2 j H(j)}{f_N(0) B [\beta^2 + (j\pi f_I / f_N(0) B)^2]}, \quad (1)$$

where f_I is the inertial frequency, $f_N(0)$ the buoyancy frequency at zero depth, B the vertical scale of the exponential ocean model and $H(j)$ the mode weighting function given by

$$H(j) = (j^2 + j_*^2)^{-1} \left/ \sum_1^{\infty} (j^2 + j_*^2)^{-1} \right. . \quad (2)$$

An appropriate value for j_* is thought to be ~ 3 , although a value of ~ 6 does not produce greatly different results. By summing over all modes, an expression can be obtained for the total horizontal spectrum at any given wavenumber. Higher modes (over 20 or so) do not contribute greatly to the total product, since the incorporated mode-weighting function decreases strongly for modes much greater than the characteristic mode j_* . The expression can then be evaluated, given values for $\langle \eta^2 \rangle$, f_I , $f_N(0)$ and B . The value of $\langle \eta^2 \rangle$ controls the absolute energy of the spectrum, but does not affect its colouring. The value of $\langle \eta^2 \rangle$ is determined by the strength of the observed inhomogeneities. f_I is fixed, given the latitude of the experiment. It remains to input sensible values for $f_N(0)$ and B . These two parameters constitute the vertical exponential part of the model. At any depth, the buoyancy frequency is modelled as

$$f_N(z) = f_N(0) \exp(-z/B), \quad (3)$$

so that these two parameters are best evaluated by fitting an exponential curve to the observed buoyancy frequency over the depth range of interest. Values of $f_N(0) = 13$ c.p.h. and $B = 100$ m result from a least error variance fit to all 10 TOB casts. The horizontal wavenumber spectrum is not very sensitive to errors in these parameters. This is because a positive error in $f_N(0)$ tend to be associated with a negative error in B (so that the buoyancy frequency decays to a sufficiently small value at large depths). The product $f_N(0)B$ is then almost invariant. In the expression for the horizontal spectrum in Eq. (1), these parameters always occur as the product.

3.3. EXPERIMENTAL RESULTS OF SEPARATION

Interpolated fields of potential density and residual sound speed were used by an inhomogeneity-splitting program, called 'waveglob'. The waveglob program used the potential density field to split the residual sound-speed field for all 10 TOB casts displayed in Fig. 7, providing 3 interpolated residual sound-speed fields; the total field, the wave field and the glob field. These fields were then used as input to a spectral analysis program which gave spectral estimates of the horizontal sound-speed variability of each field as a function of wavenumber. Spectral estimates were obtained for each 1 m depth and grouped into 6 vertical 'windows' spanning the range 40–264 m depth. The data were split into vertical windows so that the statistics would be quasi-stationary in the vertical over each window depth range. This is particularly important for the vertical analysis which follows and which we would like to compare with the horizontal analysis given here. The requirement for quasi-stationarity in the vertical must be balanced against the requirement for a large enough vertical window to resolve vertical structure. Deeper windows were expected to correspond to larger vertical length scales, requiring a longer data series over which to calculate the statistics. To achieve these joint objectives, the window size was chosen to increase exponentially with depth. The windows overlapped each other by some 50%. The window depth ranges chosen are shown in Table 2.

Table 2 *Window depth ranges*

Window (no.)	Depth range (m)	Mean depth (m)	Data length (m)
1	40–60	50	20
2	50–74	62	24
3	62–98	80	36
4	80–140	110	60
5	110–194	152	84
6	152–264	208	112

The effective horizontal resolution of the TOB at the centre depth of each window was used to truncate the spectral estimates for unrealistically high horizontal frequencies, for which estimates were made possible by the over-resolution of the interpolated field.

If the waveglob program is allowed to freely follow potential density contours to arbitrary resolution and split the sound-speed field on this basis, the spectra for the total (unsplit) field contains significantly less energy than the wave and glob field spectral energies added incoherently together, violating energy conservation. The reason for this is that the true resolution of the potential density values imposes a limit on the tolerance within which potential densities must be considered identical.

Attempts to distinguish potential densities with a finer resolution result in a 'hunting' of the potential density contour about the true depth. This generates spurious energy in the wave field, and hence also in the glob field. A second computational difficulty arises because the search is a differential operation on the density field, and therefore accentuates numerical instability.

The waveglob program was improved in two ways from the simple procedure outlined above to stabilise its output. Firstly, a smoothed vertical potential density profile was used to set contour search depth levels to improve robustness. Secondly, an interactive control was provided to adjust the resolution tolerance. If this tolerance is too low, the program 'hunts' and generates spurious energy in the wave and glob fields. If the tolerance is too high, the program fails to pick up some of the true wave displacement field and hence overestimates the glob field. The results presented here were obtained by using a tolerance value of 0.001 kg m^{-3} , a value found by trial and error. This is a low value, better than the expected resolution of the CTD sensors used in the TOB. This is justified because of the vertical filtering of the TOB data in initial data reduction, which greatly reduces instrument noise. Direct inspection of the interpolated potential density field confirms that the profiles are stable to this value.

3.4. EXAMINATION OF HORIZONTAL WAVENUMBER SPECTRA

The spectral estimates for each field were not significantly different over the 10 TOB casts. For brevity, the 30 spectral graphs, each with 6 depth windows, are not presented here. The spectral estimates for each window were averaged over all 10 TOB casts to give averaged spectral functions. Graphs of the average total, glob and wave spectral estimates for the 6 windows are given in Figs. 8a-c, together with curves evaluated from the internal-wave model developed in Subsect. 3.2.

Figure 8a shows the horizontal wavenumber spectra for the total inhomogeneity field for the 6 windows. The windows are numbered at the right side of the curves following the numbering system shown in Table 2. At all depths, the spectral shading appears to be the same, within expected errors, and is fitted well by a $\beta^{-5/2}$ spectrum, where β is the horizontal wavenumber. Overall energy levels decrease from the near-surface to 100 m. Deeper windows (100–200 m) do not show significantly different spectral energies. Both the wavenumber- and depth-dependence are not in agreement with a linear inertial-wave model, which assumes scale sizes increase exponentially with depth in the ocean.

Figure 8b shows the same spectra for the glob part of the sound-speed inhomogeneity field after separation by the program waveglob. Comparison with Fig. 8a shows that the glob field is not significantly different from the total field. The glob contribution to the total field thus appears to be overwhelmingly dominant. The observed value of $\langle \eta^2 \rangle$ over 100 m depth (4.5×10^{-9}) was used to evaluate the internal-wave model

SACLANTCEN SM-234

shown as the heavy black line. The spectral shading of the internal-wave model is seen to be significantly different from the data.

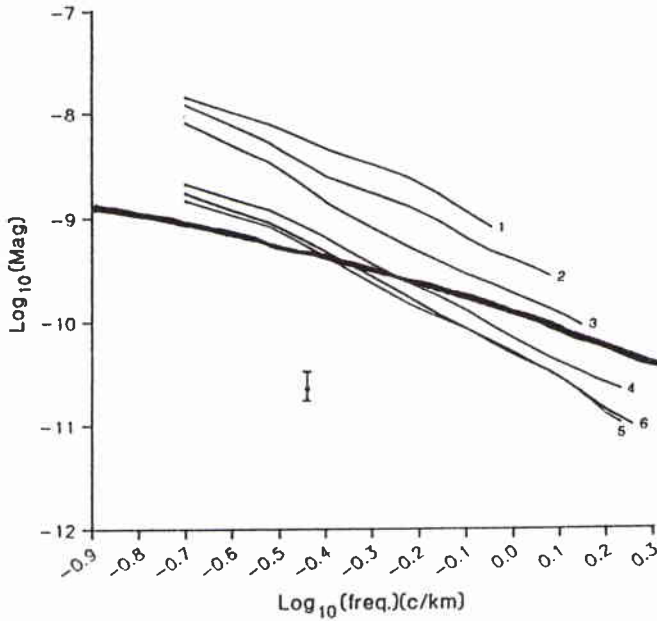


Figure 8a Average spectral energy, denoted *Mag*, of refractive index inhomogeneities against horizontal frequency, for the six depth windows described in the text over all 10 TOB casts analysed. The windows are identified by the numbers to the right of the curves. The 95% confidence limits are indicated by the vertical bar. The thick line represents values from the internal-wave model with $\langle \eta^2 \rangle = 4.5 \times 10^{-9}$. The vertical axis is scaled as $\langle \eta^2 \rangle$ per (cycle/kn).

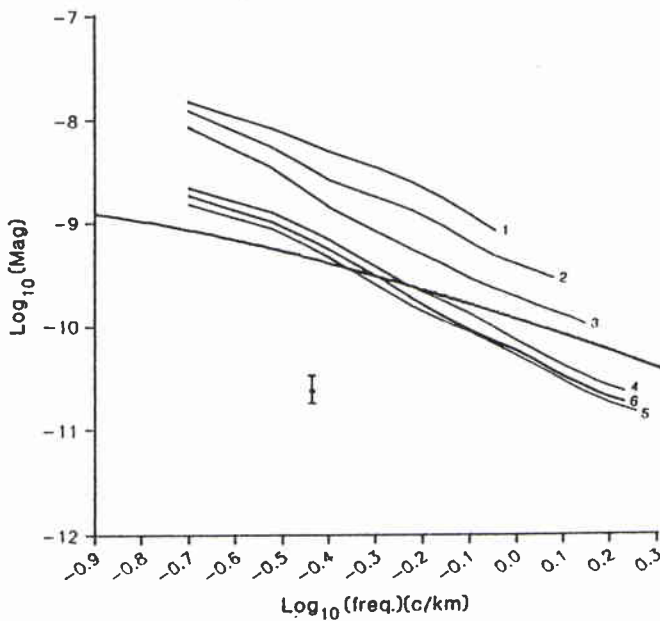


Figure 8b As for Fig. 8a but for the glob field alone.

Figure 8c shows the corresponding wave field. The energies are all much lower than for the total or glob field, except at high wavenumbers and depths over 100 m.

Even then, the internal-wave contribution is not statistically significant. In any case, the wave spectra represent an upper limit since any separation errors tend to boost the wave energy at the expense of the glob field. More striking is that the spectral shading of the wave field is markedly different than for the glob or total field. The spectra are well fitted by a $\beta^{-3/2}$ behaviour, and are in good agreement with the internal-wave model developed above. The internal-wave model, evaluated with $\langle \eta^2 \rangle = 1.25 \times 10^{-9}$, is shown as the thick unnumbered line. The agreement of internal-wave theory with the wave field, and its marked difference with the spectral shading of the glob field reinforces confidence that the glob and wave fields have been correctly separated by the waveglob program. The 'best-fit' value of $\langle \eta^2 \rangle = 1.25 \times 10^{-9}$, compared to the measured value of 4.5×10^{-9} , implies that internal waves may have contributed a maximum of some 25% of the sound-speed inhomogeneity field.

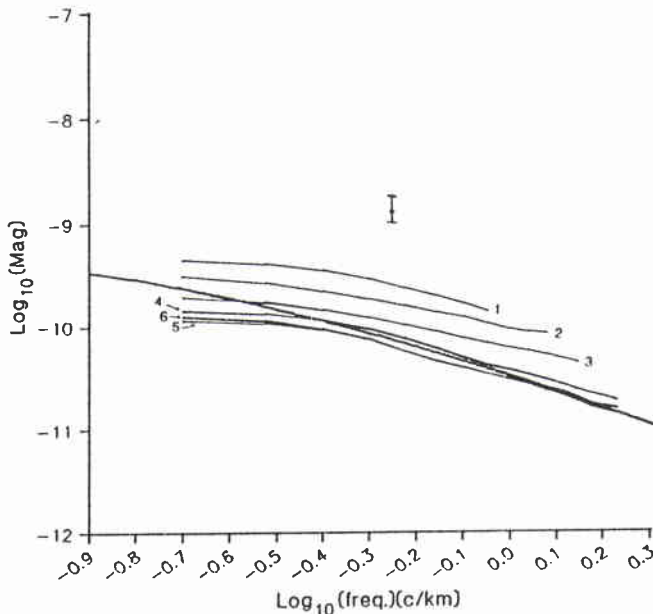


Figure 8c As for Fig. 8a but for the wave field alone and with the internal wave modelled with $\langle \eta^2 \rangle = 1.25 \times 10^{-9}$.

The clear conclusion is that internal waves (together with non-density-compensated globs) are insignificant contributors with respect to density-compensated globs as sources of sound-speed inhomogeneities over depths sampled by the TOB (40–270 m). It is possible that below 270 m, particularly at larger horizontal wavenumbers, internal-wave activity may have been significant.

Environmental characterisation

This section identifies the minimum environmental input parameters required by the acoustic scattering theory. Length scale definitions are developed and their inter-relationships explored. Length scales are evaluated in the horizontal and vertical as a function of depth. Finally, the sound-speed variance is estimated as a function of depth from TOB, CTD and XBT data.

For the purposes of applying scattering theory to the acoustic data, we have shown that internal-wave theory cannot be used. Most of the sound-speed inhomogeneities appear to be due to density-compensated globs, with only a weak depth dependence of the horizontal wavenumber spectrum. In general, the full a.c.f. of the inhomogeneities is required as input to the acoustic scattering theory. This is equivalent to evaluating the vertical and horizontal wavenumber spectra. The horizontal wavenumber spectra have already been evaluated above as a by-product of the internal-wave investigations. The vertical spectra cannot be usefully estimated because of statistical non-stationarity in the vertical data over the data lengths necessary for statistically significant spectra to be calculated. In order to avoid this difficulty, we shall assume some normalised functional form for the a.c.f. can be found and evaluate only three scalar values from the data:

- The strength of sound-speed inhomogeneities as a function of depth.
- The characteristic horizontal length scale of the random sound-speed inhomogeneities for each of the 6 depth windows.
- The characteristic vertical length scale of the random sound-speed inhomogeneities for each depth window.

The strength of the sound-speed inhomogeneities, which we shall denote by $\langle \mu^2 \rangle$, is here defined as the ensemble averaged sound-speed variance as a function of depth. The normalised functional form of the a.c.f. provides equivalent constraints to the spectral shading, shown in Sect. 3 to be empirically well fitted by a $\beta^{-5/2}$ dependence. The vertical and horizontal length scales can be combined with any assumed a.c.f. functional form as input to acoustic scattering theory, or used directly as characteristic ocean scales for many other purposes. For the latter use, we shall relate our scale definitions to other (more familiar) expressions for two model distributions, a 'boxcar' and the gaussian distribution. We shall begin by deriving values only over the TOB operating depth range. Some indication of vertical structure at greater depths can be gleaned from the CTD data and this is performed at the end of the

section, but the results are statistically weak due to the small number of casts.

4.1. LENGTH SCALES, AUTOCORRELATION AND STRUCTURE FUNCTIONS

Length scales for stochastic series can be estimated in a number of ways, one of the most popular being the $1/e$ decay length of the a.c.f.. For the purposes of the acoustic scattering theory, the length scale L_p defined by Flatté [19] is most often used for theoretical calculations:

$$L_p = \int_{-\infty}^{+\infty} \text{a.c.f.}(\zeta) d\zeta, \quad (4)$$

where henceforth ζ will denote the lag. In practice, the a.c.f. can never be calculated over infinite lags and so a direct application of this definition is not possible. In addition it is simple to demonstrate that, for a zero-mean finite data series, the sum of a.c.f. values over all possible lags is identically zero. For lags of 10% of the data length or more, this condition has the effect of artificially reducing (positive) a.c.f. values. Short data series ($< 10 \times L_p$) thus introduce a specific distortion into the a.c.f., so that even the computed $1/e$ length may be significantly in error. We would like to develop a new length scale definition which is independent of large lag a.c.f. values. We additionally require that such a replacement definition yields the same result as L_p for some simple inhomogeneity model function.

We begin by considering the simple 'boxcar' function $f(x)$ given by

$$f(x) = \begin{cases} 1, & \text{for } |x| \leq L \quad (L \text{ finite}) \\ 0, & \text{otherwise.} \end{cases} \quad (5)$$

$f(x)$ represents an inhomogeneity of obvious length $2L$. We define the function over the range $|x| \leq R$, $R > L$. In the limit as $R \rightarrow \infty$ $f(x)$ becomes zero-mean, obviating the need to mean-correct the function before calculating the a.c.f.. The normalised a.c.f. can then be expressed as

$$\text{a.c.f.}(\zeta) = \lim_{R \rightarrow \infty} \langle f(x) f(x + \zeta) \rangle / \langle f^2(x) \rangle, \quad (6)$$

where $\langle \dots \rangle$ indicate an ensemble average. Replacing the ensemble averages by integrals and restricting $\zeta \geq 0$ yields

$$\text{a.c.f.}(\zeta) = \lim_{R \rightarrow \infty} \int_{-R}^{R-\zeta} f(x) f(x + \zeta) dx / \int_{-R}^R f^2(x) dx, \quad (7)$$

which gives us the simple result

$$\text{a.c.f.}(\zeta) = \begin{cases} (2L - \zeta)/2L, & 0 \leq \zeta \leq 2L \\ 0, & \text{otherwise.} \end{cases} \quad (8)$$

Clearly the a.c.f. is symmetric about $x = 0$, so we finally obtain

$$\text{a.c.f.}(\zeta) = \begin{cases} 1 - (|\zeta|/2L), & |\zeta| \leq 2L \\ 0, & \text{otherwise.} \end{cases} \quad (9)$$

An evaluation of the integral given in Eq. (4) is then trivial and yields

$$L_p = 2L, \quad (10)$$

which is precisely the length one would naturally associate with the original boxcar input function of Eq. (5).

We would like another expression for L_p which agrees with the result of Eq. (4) for the boxcar function, but which does not require a knowledge of a.c.f. values at large ζ . Consider the derivative of the a.c.f., for the boxcar function.

$$d[\text{a.c.f.}(\zeta)]/d\zeta = -1/2L, \quad 0 \leq \zeta \leq 2L. \quad (11)$$

This result prompts us to try and define a new L_p , called L'_p , where

$$\begin{aligned} L'_p &= -d[\text{a.c.f.}(\zeta)]/d\zeta^{-1}, \\ &= L_p, \quad \text{for the boxcar function.} \end{aligned} \quad (12)$$

It is seen that the definition of L'_p is dimensionally correct and $L'_p = L_p$ for the boxcar input function, so it is possible that it provides a suitable alternative. The evaluation of L'_p requires only the initial values of the a.c.f. (ζ small) which liberates it from the infinite limit singularity encountered with applying the integral in Eq. (4). The price we have had to pay for this independence from large ζ -values is that we require the gradient of the a.c.f. to be constant for small ζ , in order for the value of L'_p to be uniquely defined. This is indeed the case for the boxcar function, but is not generally so.

It is well known that for a gaussian distributed random variable, the normalised a.c.f. is given by

$$\text{a.c.f.}(\zeta) = \exp(-\zeta^2/r^2), \quad (13)$$

where r will henceforth represent the $1/e$ scale length of the a.c.f.. Applying the definition of L'_p we obtain

$$L'_p = r^2/2\zeta \exp(\zeta^2/r^2), \quad (14)$$

which is not a constant, but a function of ζ . Since we must choose a value of ζ at which to evaluate L'_p , it seems reasonable to choose the ζ for which the resulting L'_p is most stable, i.e. where $dL'_p/d\zeta = 0$. This occurs at $\zeta = 1/\sqrt{2}r$, or only some 70%

of the $1/e$ lag, in agreement with our intention to provide a length scale definition which can be evaluated at small lags. This choice is equivalent to calculating the a.c.f. gradient where the a.c.f. curve is locally flat, an intuitively attractive option. For this lag, the calculated value of $L'_p = 1.17r$. For a gaussian distribution the scale L_p becomes

$$\begin{aligned} L_p &= \int_{-\infty}^{+\infty} \exp(\zeta^2/r^2) d\zeta, \\ &= r\sqrt{\pi}, \end{aligned} \quad (15)$$

which is some 50% larger than L'_p . In summary, we have developed a characteristic length scale definition which avoids numerically unattainable limits but which bears an uncertain relationship to L_p , depending on the type of statistical distribution. The results are summarized in Table 3.

Table 3 *Length scale relationships*

	Length scale		
	$1/e$	L_p	L'_p
boxcar function	r	$1.6r$	$1.6r$
gaussian statistics	r	$1.8r$	$1.2r$

It remains only to address the a.c.f. distortion which becomes significant when $\zeta \simeq 10\%$ of the data length. If the data length is $\geq 7r$, then the problem does not occur. For the horizontal sound-speed data, $\Rightarrow r \leq 1.4$ km, which is probably satisfied. The vertical sound-speed data, on the other hand, have strongly non-stationary statistics. Any attempt to evaluate the vertical a.c.f. either fails because of non-stationarity over the depth range considered, or because the data length is too short for the a.c.f. lags of interest.

The distortion of the a.c.f. due to finite data length can be avoided by instead considering the structure function (s.f.) given by

$$\text{s.f.}(\zeta) = \frac{1}{2} \langle [f(x) - f(x + \zeta)]^2 \rangle, \quad (16)$$

where the $\langle \dots \rangle$ symbols are used as before. Again normalising the function $f(x)$ so that its variance is unity and taking the limit as the data length goes to infinity yields

$$\text{s.f.}(\zeta) = 1 - \text{a.c.f.}(\zeta). \quad (17)$$

For finite data length, it is the a.c.f. which is distorted, not the s.f., so that we may usefully define

$$L'_p = d[\text{s.f.}(\zeta)]/d\zeta^{-1}, \quad (18)$$

SACLANTCEN SM-234

evaluated at $z = 0.7r$. This definition finally allows us to escape from both the infinite integral limits of Eq. (4) and the distortion of the a.c.f. due to finite data length. We now proceed to evaluate L'_p for the TOB data both in the horizontal and vertical. For this purpose a mean structure function was calculated for both the horizontal and vertical fields, for all six depth windows described above, in the same way as for the horizontal wavenumber spectra.

Horizontal inhomogeneity scale The average horizontal structure functions over the 10 TOB casts for the sound-speed inhomogeneity field are given in Fig. 9. The values of L'_p evaluated from Eq. (18) for the horizontal field will be denoted L_h . For these data, $r \simeq 1.2$ km. The depth dependence was too weak to warrant calculation of different values of r for different windows. Accordingly, the L_h were all evaluated at $\zeta = 850$ m. The results for the six windows are given in Table 4.

Table 4 *Horizontal length scales*

Window no.	Depth range (m)	Mean depth (m)	L_h (km)
1	40–60	50	1.5
2	50–74	62	2.0
3	62–98	80	1.6
4	80–110	110	1.9
5	110–194	152	1.9
6	152–264	208	2.0

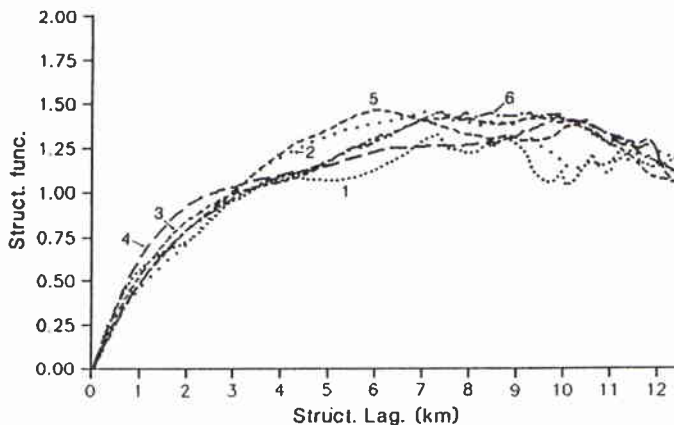


Figure 9 *Average horizontal structure functions for sound-speed inhomogeneities for the six depth windows.*

The value of L_h is rather erratic near the surface. The value of 2 km for window 2 is probably unreliable. From 100–200 m the values stabilise and no significant depth dependence is observed. On the basis of these data alone, it is dangerous to conclude

that horizontal scales will be constant below 200 m. Advective intrusions could cause anomalous regions with length scales considerably different from neighbouring areas, horizontally or vertically. This is because the advection will very often be depth limited, by density considerations, but have a horizontal scale determined by unrelated mechanisms, such as the proximity to source water. The horizontal scales associated with such globs may change rapidly over short distances, making the horizontal statistics (in addition to the vertical) non-stationary. Caution must therefore be exercised when extrapolating data into regions where no measurements have been taken.

Within the depth range of observation, we have a good indicator of the characteristic horizontal length scale which can be used in diverse ways to parameterise the sound-speed inhomogeneities in the medium. The same length scale would also serve for the purposes of salinity and temperature field characterisation.

Vertical inhomogeneity scale As with the horizontal length scale, L'_p was evaluated from the vertical TOB field to give values for L_v for the six depth windows used before. The six depth windows which we have considered in Sect. 3 were originally imposed in an attempt to ensure quasi-stationarity of the statistics for vertical calculations. Treating the TOB data exactly as for the horizontal case, we obtain the vertical structure functions for the six depth windows and these are shown in Fig. 10. A strong depth-dependence is seen. In the evaluation of the L_v , r was therefore estimated separately for each window. We then obtain the L_v values given in Table 5.

Table 5 *Vertical length scales*

Window (no.)	Depth range (m)	Mean depth (m)	r (m)	L_v (m)
1	40–60	50	4	7
2	50–74	62	5	8
3	62–98	80	7	11
4	80–140	110	7	12
5	11–194	152	9	16
6	15–264	208	14	24

L_v is much more depth-dependent than L_h . There is therefore no simple ratio of horizontal to vertical scales applicable over the entire TOB depth range. Such a ratio varies from $\sim 200 : 1$ or more near the upper limit of the TOB data to $80 : 1$ near 200 m. The trend is for the inhomogeneities to become thicker with respect to their length as depth increases. This makes intuitive sense, since globs are vertically limited by the vertical density stratification (which becomes weaker with depth), without a corresponding horizontal depth-dependent constraint. Cairns' data were

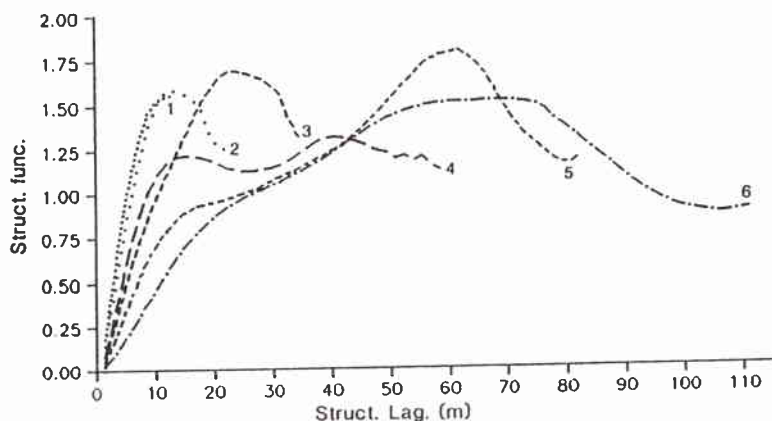


Figure 10 Average vertical structure functions for sound-speed inhomogeneities for the six depth windows.

internal-wave dominated and displayed ratios of horizontal to vertical scales from 150 : 1 down to 10 : 1 with a mean value of 50 : 1. These ratios are significantly smaller. It would be most interesting if this scale ratio could be used as an indicator to differentiate between glob and wave dominated inhomogeneities.

We would like to be able to estimate L_v at depths below 270 m, but the CTD is the only instrument which provided data with sufficient resolution below 270 m. There are only 4 CTD casts taken during the TOB measurement period, compared to the several hundred equivalent TOB oscillations. The calculation of vertical structure functions and L_v may be performed as before, but the statistical significance will clearly be very weak. The values of L_v were calculated for the six depth windows and shown to be in approximate agreement with the TOB results, with a percentage error variance of 33%. L_v was then calculated over the depth ranges 200–400 m and 300–500 m, yielding results relevant to 300 and 400 m, respectively. Assuming the percentage error variance remains the same as for shallower depths, the results are $L_v = 29 \pm 10$ m at 300 m depth and $L_v = 50 \pm 17$ m at 400 m depth. The indication is that L_v continues to increase weakly with depth.

Finally, it is useful to note that the implied values of L_p , assuming gaussian statistics, are 36 m in the vertical and 3 km in the horizontal at 208 m depth. These values may be compared directly with L_p values quoted in the multiple scattering literature (for example, see Flatté [19] or Ewart et al. [7]. In addition, Potter et al. [20] fitted an empirical model to the sound-speed inhomogeneities for these data with vertical and horizontal length scales as free parameters. The resulting values were 68 m and 6 km for the vertical and horizontal, respectively. These values are very nearly twice the L_p values, both confirming the linear relationship between the various scale definitions and providing a ratio for relating the empirical length scales found in Potter et al. [20] to values of L_p .

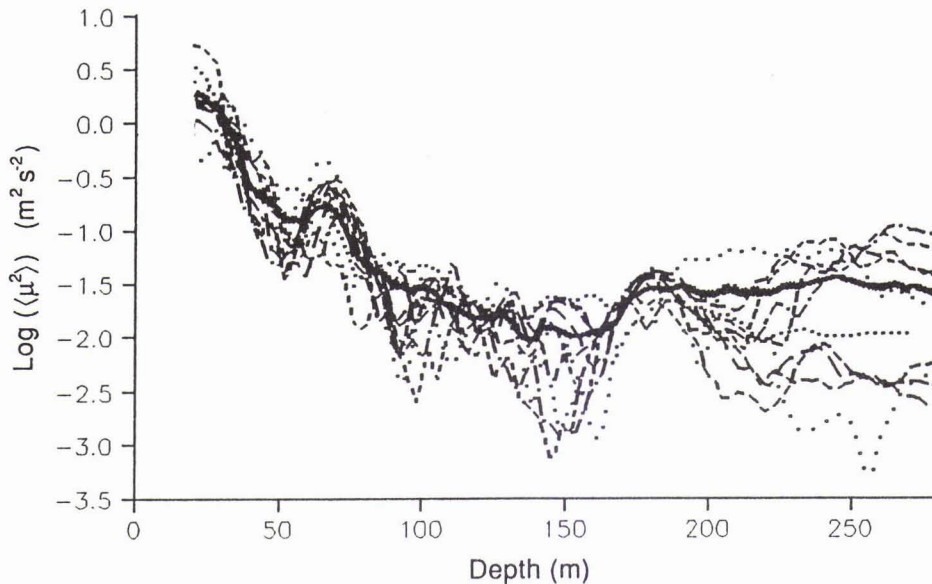


Figure 11 Sound-speed variance $\langle \mu^2 \rangle$ about the mean profile, for all 10 TOB casts. The mean curve is given by the heavy solid line.

4.2. MEASUREMENTS OF $\langle \mu^2 \rangle$, THE AVERAGED SOUND-SPEED VARIANCE

It is a relatively simple matter, once the TOB sound-speed inhomogeneity field is available, to calculate $\langle \mu^2 \rangle$ as a function of depth. The results for all the TOB casts are shown in Fig. 11 together with the mean curve over all TOB casts. There is clearly a strong trend for the variance to decrease with increasing depth, but it is by no means monotonic and there is considerable inter-cast variability. A sharp increase in the variance is seen at ~ 60 – 70 m depth, probably as a result of the high sound-speed globs observed in the casts of Fig. 7 at this depth. Some casts have a ‘hole’ in the variance at 150 m depth. In addition, the curves bifurcate into two groups at depths greater than 200 m, one group of casts encountering a sound-speed variance 10 times more than the other. This is directly attributable to the deep, low sound-speed glob discussed in the physical oceanographic analysis.

Figure 12a displays the sound-speed variances for Group A casts and Fig. 12b displays Group B casts. Within each group, the inter-cast variability is now seen to be significantly less than for all casts together. The high sound-speed variance observed at 60–70 m is observed to be due to some glob only encountered by Group A casts. The ‘hole’ at 150 m and the 200 m glob is only encountered by Group B casts. These results confirm our earlier suspicions that small (10 km or less) globs were present with lifetimes longer than the experiment and that they significantly affect the sound-speed inhomogeneity field, indeed dominate it. For globs of ~ 10 km, separated by some larger distance still, TOB casts of at least 50 km should be taken to provide an adequate statistical description. We have only isolated encounters here.

SACLANTCEN SM-234

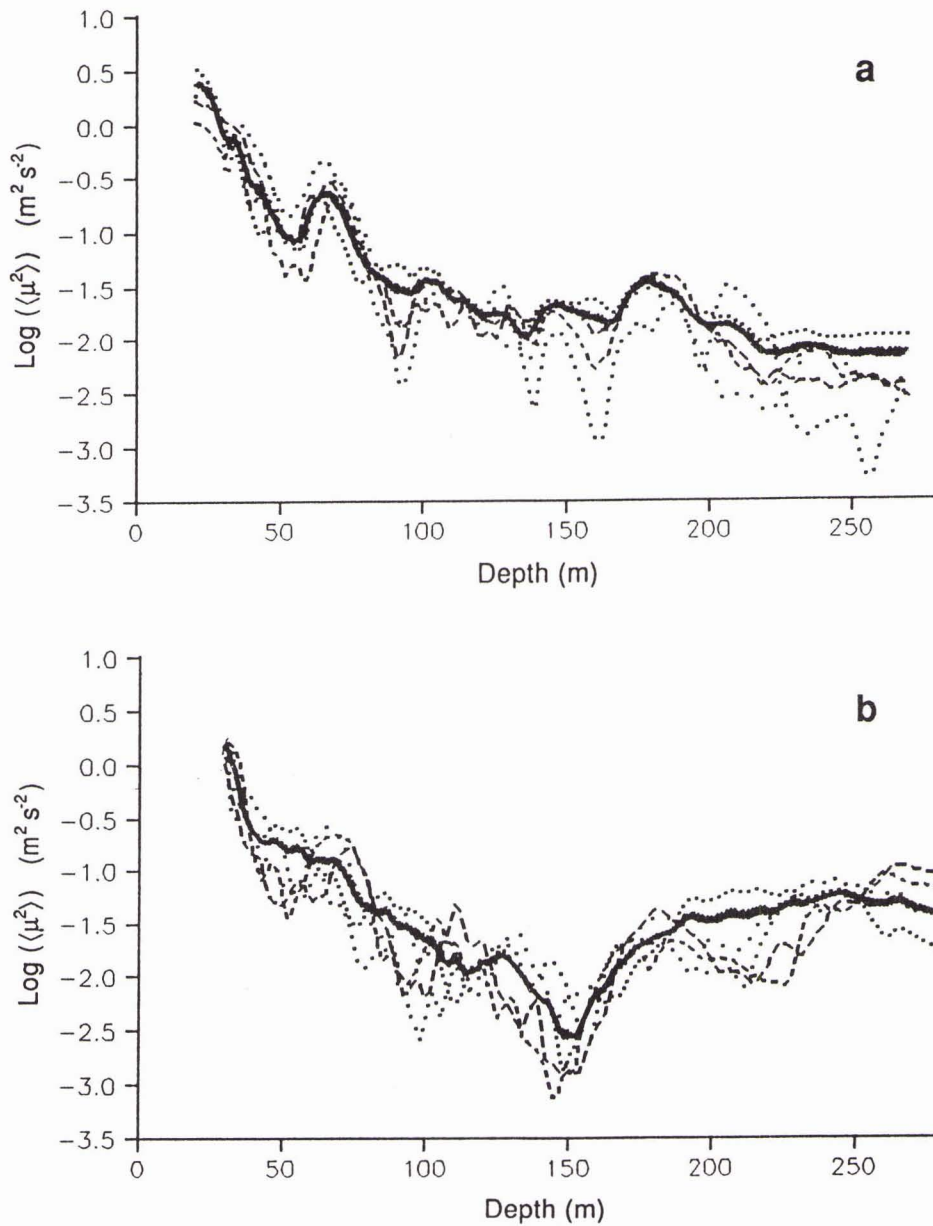


Figure 12 Sound-speed variance $\langle \mu^2 \rangle$ about the mean profile, for (a) Group A TOB casts, parallel to the acoustic propagation track, and (b) Group B TOB casts, perpendicular to the acoustic propagation track. The mean curve is given by the heavy solid line.

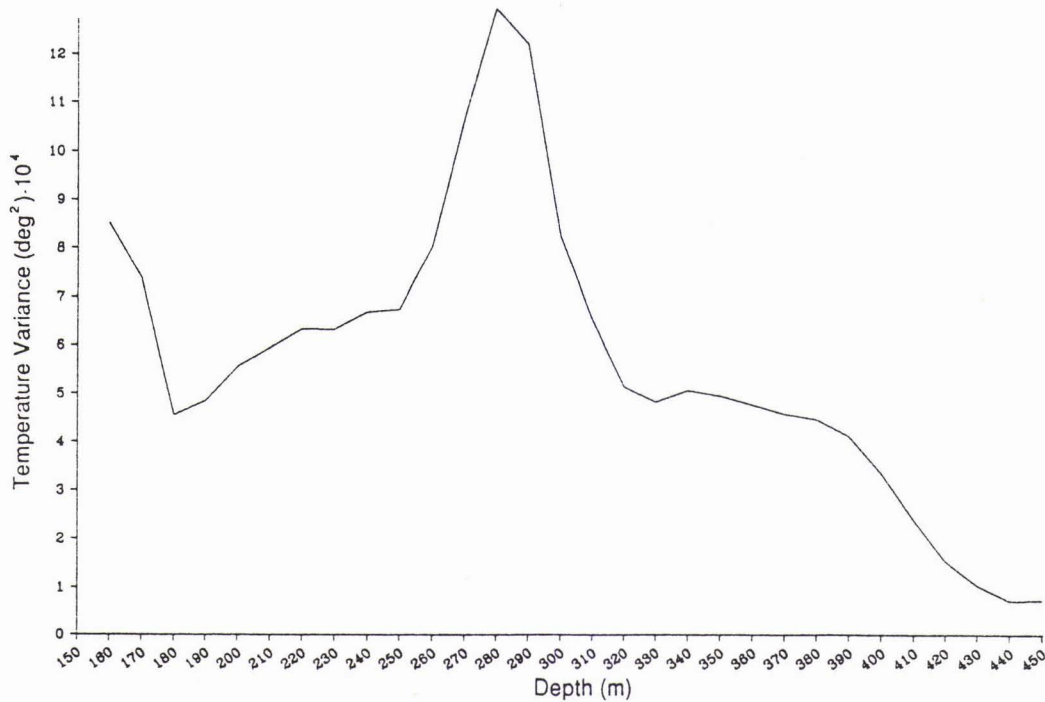


Figure 13 Temperature variance about the mean profile obtained from 59 'calibrated' XBT casts.

In order to extend the estimate of $\langle \mu^2 \rangle$ to greater depths, we wish to integrate XBT and CTD data with the TOB results. Figure 13 displays the temperature variance obtained from the XBT data after 'calibration' by the CTD data at 450 m described in the physical oceanographic analysis. Temperature, salinity and sound-speed are (to first order) linearly related (by the T - S diagram and sound-speed formula) so that trends in temperature variance accurately reflect sound-speed variance. The XBT temperature resolution is $\sim 0.02^\circ\text{C}$, giving rise to a resolved temperature variance of $4 \times 10^{-4} \text{C}^2$. This high threshold obscures all but the most prominent features at depths of 250 m or more. The only statistically significant feature is a peak from ~ 250 to 320 m depth, exceeding $3\times$ the resolution. This result is important because it represents an effect present over the entire 3-day period of the acoustic experiment, as measured by 59 XBT casts. Were such a peak to be only observed on 4 CTD casts, it could be taken for a statistical freak.

Figure 14 shows the mean sound-speed variance curves for the two TOB cast groups together with the CTD sound-speed variance. A mean curve (heavily weighted to favour the TOB data where they are available) is also shown. It is seen that, above 270 m depth, the CTD data follow the Group A TOB casts, parallel to the acoustic path. This is unsurprising, since the MPG, at one end of the acoustic path, made the CTD casts. Below 270 m, where no TOB data are available, the CTD variance rises rapidly, showing the peak revealed by the XBT data and matching the level obtained by the Group B TOB casts. The inference is that the glob discernible in

SACLANTCEN SM-234

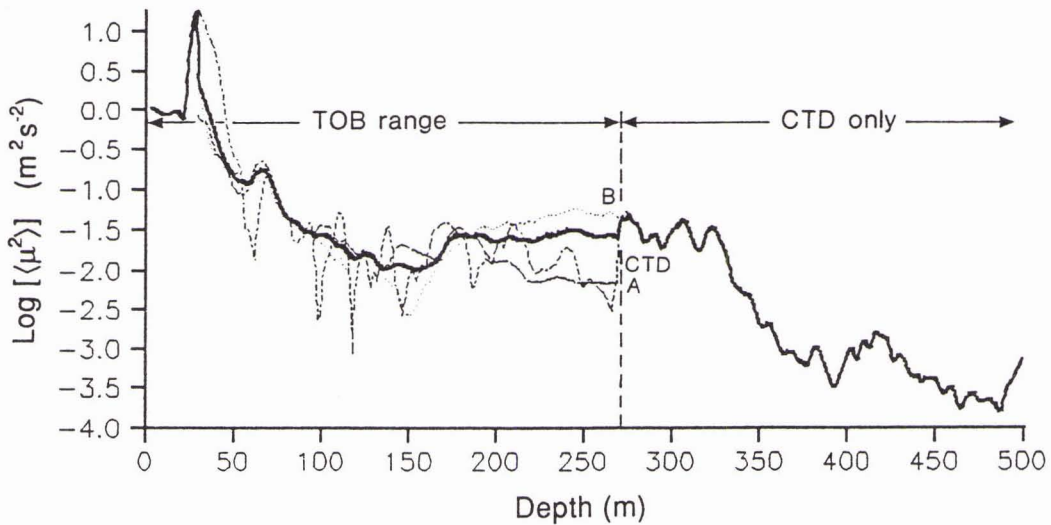


Figure 14 Mean sound-speed variance ($\langle \mu^2 \rangle$) for Groups A and B TOB casts and 4 CTD casts. The mean curve is given by the heavy solid line.

the Group B TOB casts at ~ 250 m had a neighbour, lying below the MPG for at least some of the 3 days, extending from some 270 to 320 m depth. The deeper glob may be due to LIW but is more likely to be a similar water mass as the shallower glob, since it causes the same sound-speed variance, which is determined by the temperature and salinity contrast between the glob water mass and the background water type.

The resulting mean curve, obtained from an amalgamation of TOB, XBT and CTD data, shows the high-variance plateau from 180 to 320 m depth, resulting from intrusive globs. Except for this plateau (also observed with the XBT's), below 275 m the small number of CTD casts makes interpretation unreliable.

5

Conclusions

The environmental data collected during NAPOLI '85 have provided a wealth of detail concerning both the dynamic oceanographic environment and the acoustic propagation environment. The most important result is that inhomogeneities in the ocean medium were dominated by detached intrusions of a different water mass from the background water type, not by internal wave activity. Analysis methods have been developed to identify and treat this situation. Some peripheral results concerning identification and tracking of these intrusions, or globs, were obtained and showed that 2-D sections of the ocean are essential in order to correctly characterise the environment for acoustic propagation purposes. Some first steps in this characterisation have been made by using structure functions, instead of autocorrelation functions, and in defining length scales. Some inviting possibilities have surfaced as a result of the successful tracking of several oceanic features over many casts.

References

-
- [1] Uscinski, B.J. Intensity fluctuations in a multiple scattering medium. Solution of the fourth moment equation. *Proceedings of the Royal Society*, **A 380**, 1982: 137–169.
 - [2] Potter, J.R. and Miller, S. Some recent experiments on acoustic fluctuations in the sea. In: Dobbins, P., ed. Fluctuation phenomena in underwater acoustics, 9–10 December 1986, Weymouth, England. *Proceedings of the Institute of acoustics*, **8(5)**, 1986: 144–152.
 - [3] de Strobel, F. New oceanographic tools at SACLANTCEN. SACLANTCEN CP-19. La Spezia, Italy. SACLANT Undersea Research Centre, 1978.
 - [4] Phin, L. The analysis of oceanic stochastic inhomogeneities using physical data. SACLANTCEN IN-657. La Spezia, Italy. SACLANT Undersea Research Centre, 1987. (Unpublished manuscript.)
 - [5] Williams, R.B. The AIM project: Internal waves and microstructure in the thermocline and their effects on acoustic propagation. SACLANTCEN SM-126. La Spezia, Italy. SACLANT Undersea Research Centre, 1979.
 - [6] Garrett, C.J.R. and Munk, W.H. Space-time scales of internal waves. *Geophysical Fluid Mechanics*, **2**, 1972: 225–264.
 - [7] Ewart, T.E., Macaskill, C. and Uscinski, B.J. The MATE acoustic cross-correlation of intensity. *Journal of the Acoustical Society of America*, **77**, 1985: 1732–1741.
 - [8] Ewart, T.E., Macaskill, C. and Uscinski, B.J. Intensity fluctuations. Part II: Comparison with the Cobb experiment. *Journal of the Acoustical Society of America*, **74**, 1983: 1484–1499.
 - [9] Cairns, J.L. Variability in the Gulf of Cadiz: Internal waves and globs. *Journal of Physical Oceanography*, **10**, 1980: 579–595.
 - [10] Ewart, T.E. and Reynolds, S.A. The Mid-Ocean Acoustic Transmission Experiment, MATE. *Journal of the Acoustical Society of America*, **75**, 1984: 785–802.
 - [11] Johannessen, O.M. and Lee, O.S. Thermohaline staircase structure in the Tyrrhenian Sea. *Deep-Sea Research*, **21**, 1970: 629–639.
 - [12] Molcard, R. and Tait, R.I. The steady state of the step structure in the Tyrrhenian Sea. SACLANTCEN SR-24. La Spezia, Italy, SACLANT Undersea Research Centre, 1978.
 - [13] Hopkins, T.S. and Zanasca, P. Oceanographic data from the southern Tyrrhenian Sea: August to October 1984, Part 1: Floats and moored instruments, Part 2: Hydrography. SACLANTCEN SM-198. La Spezia, Italy, SACLANT Undersea Research Centre, 1988.
 - [14] Johnson, C.L., Cox, C.S. and Gallagher, B. The separation of wave-induced and intrusion oceanic finestructure. *Journal of Physical Oceanography*, **8**, 1978: 846–860.
 - [15] Gregg, M.C., Cox, C.S. and Hacker, P.W. Vertical microstructure measurements in the central North Pacific. *Journal of Physical Oceanography*, **3**, 1973: 458–469.
 - [16] Delnore, V.E. Numerical simulation of thermohaline convection in the upper ocean. *Journal of Fluid Mechanics*, **96**, 1980: 803–826.

- [17] Garrett, C.J.R. and Munk, W.H. Space-time scales of internal waves: a progress report. *Journal of Geophysical Research*, **3**, 1975: 291–297.
- [18] Munk, W.H. and Zachariassen, F. Sound propagation through a fluctuating stratified ocean: theory and observation. *Journal of the Acoustical Society of America*, **59**, 1976: 818–838.
- [19] Flatté, S.M., *ed.* Sound transmission through a fluctuating ocean. Cambridge, UK, Cambridge University Press, 1979.
- [20] Potter, J.R., Akal, T. and Uscinski, B.J. Transmission-time variability, vertical spatial and temporal analysis of NAPOLI '85, an experiment in the Tyrrhenian Sea. SAC-LANTCEN SM-223. La Spezia, Italy, SACLANT Undersea Research Centre, 1989.

Initial Distribution for SM-234

Ministries of Defence

JSPHQ Belgium	2
DND Canada	10
CHOD Denmark	8
MOD France	8
MOD Germany	15
MOD Greece	11
MOD Italy	10
MOD Netherlands	12
CHOD Norway	10
MOD Portugal	5
MOD Spain	2
MOD Turkey	5
MOD UK	20
SECDEF US	60

NATO Authorities

NAMILCOM	2
SACLANT	3
CINCIBERLANT	1

SCNR for SACLANTCEN

SCNR Belgium	1
SCNR Canada	1
SCNR Denmark	1
SCNR Germany	1
SCNR Greece	1
SCNR Italy	1
SCNR Netherlands	1
SCNR Norway	1
SCNR Portugal	1
SCNR Spain	1
SCNR Turkey	1

SCNR UK	1
SCNR US	2
SECGEN Rep. SCNR	1
NAMILCOM Rep. SCNR	1

National Liaison Officers

NLO Canada	1
NLO Denmark	1
NLO Germany	1
NLO Italy	1
NLO Netherlands	1
NLO UK	1
NLO US	1

NLR to SACLANT

NLR Belgium	1
NLR Canada	1
NLR Denmark	1
NLR Germany	1
NLR Greece	1
NLR Italy	1
NLR Netherlands	1
NLR Norway	1
NLR Portugal	1
NLR Turkey	1
NLR UK	1

Total external distribution	218
SACLANTCEN Library	10
Stock	32
<hr/>	
Total number of copies	260